ELSEVIER

Thermochimica Acta 304/305 (1997) 67–98

thermochimica acta

Progress in experimental techniques for dynamic calorimetry

Yoon-Hee Jeong*

Department of Physics, Pohang University of Science and Technology, Pohang, Kyungbuk 790-784, South Korea

Received 31 July 1996; accepted 29 January 1997

Abstract

The dynamic heat capacity of a substance is a fundamental quantity related to the dynamics of the material and its measurement provides invaluable information on the system dynamics. We developed dynamic calorimeters based on the temperature modulation method and the adiabatic method. These dynamic calorimetric techniques were applied to the study of slow relaxation of a supercooled liquid $[Ca(NO_3)_2]_{0.4}(KNO_3)_{0.6}$ near the glass transition. After defining dynamic heat capacity from the linear response theory, we describe theoretical as well as technical aspects of modulation calorimeters and adiabatic calorimeters developed in this laboratory in detail. Based on the dynamic heat capacity data of calcium-potassium nitrate obtained with these calorimeters, merits and demerits of the various methods are pointed out. Future prospects are given.

Keywords: Adiabatic calorimeter; Dynamic calorimetry; Dynamic heat capacity; Glass transition; Modulation calorimeter; Relaxation

1. Introduction

Calorimetry, whose name originates from Lavoisier's caloric theory of heat [1], is an indispensable tool for modern day research in chemistry, physics, materials science, and biology, and a number of methods with varying degrees of precision and accuracy have been developed [2]. This is due to the fact that it allows one to directly monitor the free energy change of a given system as the external parameter such as temperature varies. This unique ability of calorimetry follows from the definition that heat capacity (per unit volume), C_p, is given thermodynamically by

$$C_p = \frac{1}{V}\frac{dH}{dT} = \frac{T}{V}\frac{dS}{dT} \quad (1)$$

where T, H, S, V are the temperature, the enthalpy, the entropy, and the volume of a given system, respectively [3]. One of the common experimental methods used to probe a condensed matter system is to measure the linear response of the system to a small external perturbation; heat capacity represents how the temperature of the system varies when a small amount of external heat is applied to it. Dielectric constant is another example belonging to the same class; dielectric constant represents the response of the system to a small external electric field. While it is well known that dielectric constant may be frequency-dependent,

*yhj@postech.ac.kr

0040-6031/97/$17.00
PII S0040-6031(97)00091-9

it is less well known that heat capacity may be a dynamic quantity.

Since heat capacity is generally considered to be a static thermodynamic quantity as defined above, the concept of *dynamic heat capacity* seems, at first glance, perplexing. However, the concept of dynamic heat capacity appears natural if one recalls that static thermodynamic quantities are time-averaged (or ensemble-averaged) ones. In other words, they are static not because they do not change in time, but because they change too rapidly on the experimental time scale. Consequently, it is quite conceivable that there exists a situation where the value of heat capacity depends on the measuring time scale. (We shall use the term dynamic heat capacity to denote frequency or time dependent heat capacity. See Section 2.1.) Suppose, for instance, a system contains a slow process relaxing with a characteristic time τ which lies within our experimental time window, then this will result in the complex frequency-dependent heat capacity, $C_p(\omega)$. $C_p(\omega)$ of this system would show dispersion in real part and a peak in imaginary part at $\omega \approx \tau$ just in the same way as dielectric constant does. Indeed, this idea of dynamic heat capacity has already been suggested long ago in the literature. Anomalous ultrasonic attenuations in polyatomic gases [4] and the critical attenuation of ultrasound near critical points [5], for instance, have been explained in terms of dynamic heat capacity. Although it is not common to directly observe dynamic heat capacity, there are experimental situations where these dynamic heat capacities were indeed measured. For example, Smith [6] observed the frequency dependent heat capacity in germanium and discussed it in terms of a delay in equilibrium. Dynamic heat capacity due to structural relaxation was also measured near the glass transition of glycerol [7], salol [8], potassium–calcium nitrate mixture [9,10], and polymers [11].

In this paper, we review our efforts to develop calorimetric techniques to *directly* measure the dynamic heat capacity of condensed matter. We shall call these calorimetric techniques collectively *dynamic calorimetry*. Our efforts have been directed in two directions: the temperature modulation method and the adiabatic method. A modulation calorimeter measures the response of a sample to a small oscillatory heat input. Thus, one works in the frequency domain in modulation calorimetry and the inverse of the oscillation frequency sets a natural experimental time scale. An adiabatic calorimeter, on the other hand, works in the time domain; one applies a heat pulse to a sample and follows the temperature change of the sample as a function of time. Data obtained by modulation and adiabatic calorimeters are connected to each other via the Fourier transform. We have also developed a method for operating the adiabatic calorimeter in the scanning mode (cooling as well as heating) with variable scanning rates from 0.01 to 2 K/min. These various dynamic calorimetric techniques are described in what follows; however, commercially available calorimeters, which can yield dynamic information, such as differential scanning calorimeters (DSC) and modulated temperature DSC (MTDSC) are not discussed here, since they are treated elsewhere in this issue.

The organization of the paper is as follows: In Section 2, we present a brief theory for dynamic heat capacity from a phenomenological point of view and discuss the general aspects of dynamic calorimetry. Then in the following sections, we describe in detail the principles of dynamic calorimeters we constructed and the experimental implementation of the principles. The discussion of each method is closed with experimental results obtained by applying the method to our standard sample, a supercooled liquid $[Ca(NO_3)_2]_{0.4}(KNO_3)_{0.6}$(CKN). When a liquid is supercooled without crystallization, a slow relaxation phenomenon occurs and the dynamic heat capacity can be observed. CKN, a binary mixture which becomes an ionic liquid when melted, is one of canonical glass-formers and will play a role of testing ground for our various dynamic calorimetric techniques. Since potassium and calcium ions have spherical charge distributions and nitrate ions are of trigon shape, CKN represents one of simple systems which can stay undercooled for days without crystallization. It is the point of this paper to display the capability of dynamic calorimetry as a dynamic probe of condensed matter, so that we refrain from presenting a variety of data from diverse physical systems. However, dynamic calorimetry has wide potential applications; this point and future outlooks are discussed in the final section.

2. Dynamic heat capacity and dynamic calorimetry

2.1. Linear response theory

To extend the thermodynamic definition of heat capacity given in Eq. (1), we resort to the general response equation [12]: The response $\epsilon(t)$ of a system to an external perturbation $\sigma(t)$ can be written as

$$\epsilon(t) = \int_{-\infty}^{t} K_1(t,t')\sigma(t')\mathrm{d}t' + \int_{-\infty}^{t}\int_{-\infty}^{t} K_2(t,t',t'')\sigma(t')\sigma(t'')\mathrm{d}t'\mathrm{d}t'' + \ldots \tag{2}$$

Here ϵ is any strain quantity, σ is an externally applied stress quantity, and K_1 and K_2 represent the response functions. Eq. (2) was derived under only two assumptions, *causality and analyticity*, [13] and therefore is applicable to a variety of linear and nonlinear situations. From the statistical mechanical point of view, all the equilibrium or near-equilibrium properties of a system with a fixed volume are described as a function of $\mathscr{H}_0/k_\mathrm{B}T$, where $\mathscr{H}_0$ is the Hamiltonian of the system and k_B is the Boltzmann constant. For a small temperature variation δT, the perturbing term in the Hamiltonian can be obtained from

$$\frac{\mathscr{H}_0}{k_\mathrm{B}(T+\delta T)} \approx \frac{\mathscr{H}_0(1-\delta T/T)}{k_\mathrm{B}T}. \tag{3}$$

Thus, the external perturbing field σ, in our case, is represented by $\delta T/T$ which couples to the Hamiltonian of the system in the fixed volume case. For isobaric situations which is more common with condensed matter, $\delta T/T$ couples to $(\mathscr{H}_0 + pV)$ where p denotes pressure. Except for phenomena occurring at low temperatures $\delta T/T$ is usually small and thus only the first term in Eq. (2) is necessary and one can utilize the linear response theory [14].

For the isobaric thermal responses ϵ is equal to the enthalpy change from the equilibrium value, $\delta\langle H\rangle$, per unit volume and Eq. (2) becomes [15]

$$\frac{\delta\langle H(t)\rangle}{V} = \int_{-\infty}^{t} K_H(t,t')\delta T(t')\mathrm{d}t' + C_\mathrm{p}^{\infty}\delta T(t). \tag{4}$$

Here we have taken δT as the perturbation instead of $\delta T/T$ following the usual definition of the heat capacity. C_p^{∞} represents the contribution from the fast degrees of freedom such as phonons and K_H is the response function due to the slow relaxation of the system. One also defines the relaxation function

$$R(t,t') = \int_{-\infty}^{t'} K_H(t,t'')\mathrm{d}t'' \tag{5}$$

which represents the response of the system to a step-like stimulus. For the system in equilibrium the relaxation function has the property of being stationary, that is, $R(t,t') = R(t-t')$. Then from the linear response theory, it can be shown that

$$R(t) = \frac{\langle \delta H_R(t)\delta H_R(0)\rangle}{k_\mathrm{B}T^2V} \tag{6}$$

where δH_R represents the enthalpy fluctuation associated with the slow relaxation.

In the frequency domain [16], that is, with the oscillating perturbation $\delta T \sim \exp(i\omega t)$, the dynamic heat capacity with real and imaginary parts, $C_\mathrm{p}(\omega) = C_\mathrm{p}'(\omega) - iC_\mathrm{p}''(\omega)$, may be expressed in terms of the one-sided Fourier transform of either the response function $K_H(t)$ or the time derivative of the relaxation function $R(t)$ from Eq. (4) [17]:

$$C_\mathrm{p}(\omega) = \int_0^{\infty} K_H(t)\mathrm{e}^{-i\omega t}\mathrm{d}t + C_\mathrm{p}^{\infty} = \int_0^{\infty} [-\mathrm{d}R(t)/\mathrm{d}t]\mathrm{e}^{-i\omega t}\mathrm{d}t + C_\mathrm{p}^{\infty}. \tag{7}$$

Since $R(t)$ is given by the enthalpy–enthalpy correlation function, $C_\mathrm{p}(\omega)$ can be written as

$$C_\mathrm{p}(\omega) = C_\mathrm{p}^{0} - \frac{i\omega}{k_\mathrm{B}T^2V}\int_0^{\infty} \mathrm{d}t\,\mathrm{e}^{-i\omega t}\langle \delta H_R(0)\delta H_R(t)\rangle \tag{8}$$

where C_p^{0} is the usual static heat capacity given by

$$C_\mathrm{p}^{0} = C_\mathrm{p}^{\infty} + R(0) = C_\mathrm{p}^{\infty} + \frac{\langle \delta H_R^2\rangle}{k_\mathrm{B}T^2V}. \tag{9}$$

Thus, the slow relaxation of enthalpy governed by the system dynamics is the origin of the frequency-depen-

dent heat capacity and therefore one can probe the slow dynamics of the system by measuring the dynamic specific heat. On the other hand, when the dynamics of the system occurs at a rate faster than the probing frequencies, then the dynamic heat capacity becomes the usual static heat capacity.

2.2. Examples of dynamic heat capacity

In this section a very simple model illustrating dynamic heat capacity, originally due to Herzfeld and Rice [4], is presented for the heuristic purpose. Elementary aspects of glass transition related to dynamic heat capacity are also discussed. Early studies of sound propagation in gases revealed a striking, then unexpected difference in the attenuation constant between monoatomic gases and polyatomic gases [18]. The sound absorption in CO_2, for instance, shows a peak at about 20 kHz at 1 atmospheric pressure. Since, the physics of gases are governed by collisions and the collision time τ_c is approximately 10^{-10} s under STP, one would expect only monotonic behaviors at such low frequencies. Herzfeld and Rice pointed out that the absorption peak in a polyatomic gas could be explained by the thermal relaxation caused by the temperature oscillation accompanying adiabatic sound propagation in the gas.

Suppose a certain amount of heat pulse is given to a gas system, say O_2, then this energy will be distributed among different degrees of freedom for the system to achieve equilibrium. Energy transfer between different degrees of freedom in gas molecules takes place via collisions. Since the efficiency of energy transfer among translational (and rotational), or external, degrees of freedom is very effective, it only takes several collisions to establish equilibrium. It also turned out that the energy exchange between vibrational degrees of freedom in polyatomic molecules can proceed rapidly; thus, it takes only several hundred collisions for the vibrational, or internal, degrees of freedom to establish equilibrium among themselves. On the other hand, the energy transfer efficiency between external and internal degrees of freedom is very poor and it may take millions of collisions for the system to fully equilibrate. Thus one can model the polyatomic system as consisting of two distinct, that is, external and internal, thermodynamic systems with their own, possibly

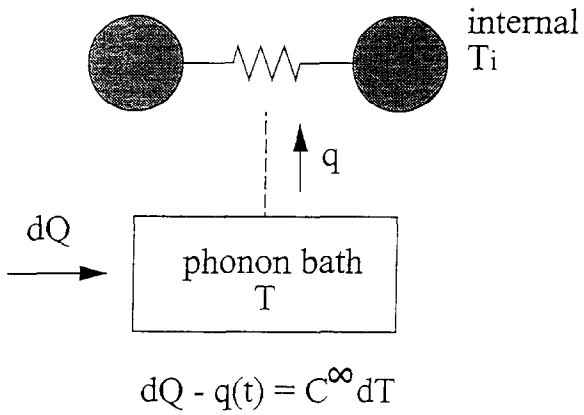

Fig. 1. Schematic diagram representing a polyatomic gas system. The translational degrees of freedom is designated as phonon bath (in the context of condensed matter) and its temperature is denoted by T. The internal degrees of freedom are depicted by a spring in the dumbbell-shaped object in the figure; however, the object represents not a single molecule, but all the molecules collectively. The internal degrees of freedom are at T_i called internal temperature. There occurs a heat flow q, characterized by the relaxation time τ, from the phonon bath to the internal degrees of freedom, when dQ is given to the system. C^∞ is the heat capacity of the phonon bath.

different, temperatures. (We regard that the two systems establish their respective equilibriums instantaneously.)

A schematic diagram depicting the model is shown in Fig. 1. We call the external degrees of freedom collectively as the phonon bath; its temperature and heat capacity are denoted by T and C^∞, respectively. (Since our main concern is on condensed matter in this paper, the term *phonon bath* is used to designate instantly responding degrees of freedom.) It should be kept in mind that the temperature we detect with a sensor is the phonon temperature T and this is what appears in the response equation Eq. (4). (See Section 2.3.) The situation is described by the energy balance equation:

$$dQ - q(t) = C^\infty dT \tag{10}$$

where dQ is the energy input to the phonon bath and $q(t)$ is the energy flow from the phonon bath to the internal degrees of freedom. The latter process is assumed to be characterized by the relaxation time τ. By defining the internal heat capacity $C^i = dq/dT_i$ where T_i is the internal temperature and using a typical

relaxation equation for T_i

$$\frac{dT_i}{dt} = -\frac{T_i - T}{\tau}, \tag{11}$$

Eq. (10) is turned into the rate equation

$$C^{\infty}\frac{dT}{dt} = \frac{dQ}{dt} + C^{i}\frac{T_i - T}{\tau}. \tag{12}$$

Remembering that Eq. (12) is a linear equation, we write, for an oscillating heat input $Q = Q_0 \exp(i\omega t)$, the temperature oscillations as

$$T = \delta T^{*} e^{i\omega t} + T_0;\ T_i = \delta T_i^{*} e^{i\omega t} + T_0 \tag{13}$$

where T_0 is the equilibrium temperature and δT^{*} and δT_i^{*} are the complex amplitudes of oscillation. Then Eq. (11) yields

$$\delta T_i^{*} = \frac{\delta T^{*}}{1 + i\omega\tau}, \tag{14}$$

and the complex dynamic heat capacity, $C(\omega) \equiv Q_0/\delta T^{*}$, is given from Eq. (12) by

$$C(\omega) = C^{\infty} + \frac{C^{i}}{1 + i\omega\tau} = C^{0} - C^{i}\frac{i\omega\tau}{1 + i\omega\tau} \tag{15}$$

where $C^{0} = C^{\infty} + C^{i}$ is the static heat capacity. Thus, this simple model with the Debye relaxation clearly illustrates what lies at the heart of dynamic heat capacity. It typically occurs when two or more thermodynamic systems, which are parts of one physical system, are not in (global) equilibrium but relaxing toward equilibrium, although they themselves are in local equilibrium separately.

Of course, there exist many such examples in condensed matter: ions and electrons in a plasma system; hot electrons in a semiconductor; spin and lattice degrees of freedom in nuclear magnetic resonance; and two level systems in a glass at low temperatures to name a few [19]. However, the relaxation times of these phenomena are generally very short and consequently dynamic heat capacity is not directly observable. Glass transition phenomenon provides a good example of dynamic heat capacity. When a liquid is cooled below its freezing point, it normally crystallizes within a few degrees of supercooling. But for some materials, so-called good glass-formers, a large degree of supercooling is possible and the slow dynamics of the supercooled state can be studied with dynamic calorimetry whose practical dynamic range is from 10^{-2} Hz to several kHz. As a glass former is cooled below its freezing point, the characteristic time of the relaxing internal modes gets longer and at some point the relaxing modes split off from other fast degrees of freedom which set the system temperature, T. Although it is not clear what constitutes the internal modes in a supercooled liquid, it is still possible to deal with this situation in a phenomenologically simple way by defining the temperature for the internal modes just as it was done in the polyatomic gas case. This internal temperature is usually called *fictive* temperature T_f in the literature [20]. The dynamic heat capacity associated with supercooled liquids turned out to have very different shape from the simple Debye form, indicating the collective nature of glass transition phenomenon.

2.3. General aspects of dynamic calorimetry

In this section, we briefly consider the general aspects of dynamic calorimetry in connection with Eq. (4); technical details of various methods are described in the following sections. It should be pointed out that there are two methods of measuring the dynamic heat capacity of a given system using Eq. (4). First, one may generate a temperature oscillation in the system by thermally attaching the system to a heat reservoir whose temperature is oscillating, and measure the response $\delta\langle H\rangle$. (The time domain version or a temperature jump experiment can be conducted in a similar fashion.) The variation of the enthalpy of the system can be monitored by watching the heat flow $\dot{Q}_{fl}$ from the reservoir to the system, since $\delta\langle H\rangle = \int dt \dot{Q}_{fl}$ by the first law of thermodynamics. This is the method used in DSC or MDSC measurements where power is varied according to the prescribed temperature variation. The converse situation occurs in the second method: one supplies an oscillating heat (or a known fixed amount of heat) to the system and monitors the ensuing temperature response with a sensor. All the calorimeters we describe in this paper adopt the second method.

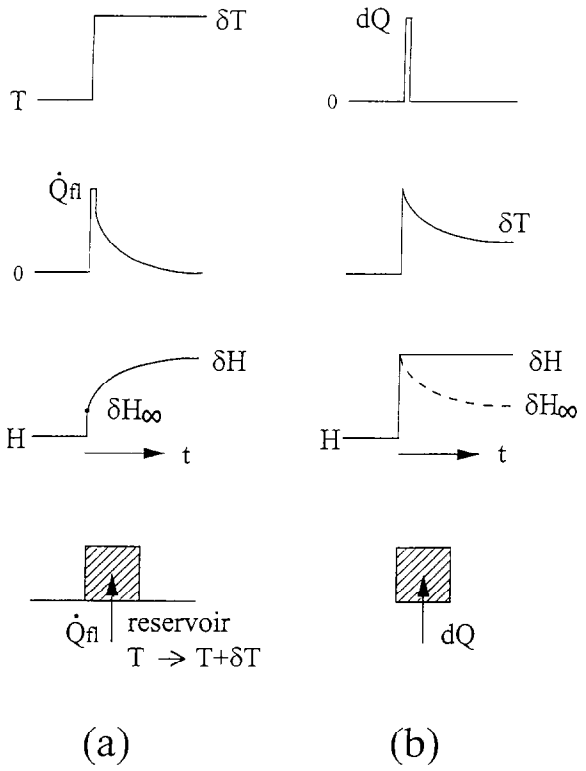

Fig. 2. Schematic diagrams showing two methods of measuring dynamic heat capacity: (a) The system is thermally attached to the reservoir and the temperature of the reservoir jumps from T to $T + \delta T$ at a certain instant as depicted in the top figure. The heat flow $\dot{Q}_{fl}$ from the reservoir to the system behaves as described in the second figure. An instantaneous heat absorption, corresponding to δH_∞, by the fast degrees of freedom is followed by the gradual heat flow caused by the absorption of the slow degrees of freedom. (b) A certain amount of heat, dQ, is given to the system as sketched in the top figure, and the change in the system temperature T is followed. The system temperature T jumps instantaneously, and this instantaneous jump is accompanied by the gradual decrease as the supplied heat energy is shared by the internal degrees of freedom. The decrease in δH_∞ appears as an increase in the internal enthalpy δH_R by the same amount.

Perhaps it is more instructive for understanding the above two views if one considers the response of the system in the time domain, rather than in the frequency domain. Fig. 2(a) is a schematic diagram depicting the first method, where the system is in intimate contact with the reservoir. Now suppose that there is a step-like temperature jump δT in the reservoir. The same δT shift is established in the system temperature via the heat flow from the reservoir to the system. If one carefully analyze $\dot{Q}_{fl}$ as a function of time, one will find that it consists of two parts: the instantly responding part, $\dot{Q}_{fl}^{\infty}$; and the slowly responding part, $\dot{Q}_{fl}^{int}$. In other words, the system takes up $Q_{fl}^{\infty} = \int dt \dot{Q}_{fl}^{\infty}$, which is due to the fast degrees of freedom (external or phonon), and brings up its temperature (or more accurately its phonon temperature) by δT instantly. However, it takes time for its internal degrees of freedom to respond and they will absorb $\dot{Q}_{fl}^{int}$ gradually from the reservoir to reach equilibrium. From this discussion it is clear that what we call the temperature of the system is that of the external degrees of freedom of the system when it is not in full equilibrium. Fig. 2(b) depicts the opposite situation where a constant amount of heat is supplied to the system and the temperature of the system is followed. Here at the instant when heat is supplied the energy is shared only among the phonon degrees of freedom, and then part of energy slowly diffuses into the internal degrees of freedom. Thus, the temperature of the system (again more accurately its phonon temperature) first shows a step-like jump which is then followed by a gradual decrease as shown in Fig. 2(b). In closing this section we mention one aspect of heat which was neglected in the discussion, but is practically very important in constructing calorimeters. That is, heat does not propagate, but diffuse. It means that one cannot raise the temperature of a whole sample of any finite size instantly and the process must involve thermal conduction and consequently thermal conductivity of the sample. Although thermal conductivity is in its own right very important physical quantity, it can become a nuisance in measuring dynamic heat capacity.

2.4. *Physical meaning of the imaginary part* $C_p''(\omega)$

One of the interesting aspects of generalizing heat capacity defined in Eq. (1) to a dynamic quantity as defined in Eq. (8) is the appearance of the imaginary part in dynamic heat capacity. At first glance this may seem strange in view of the facts that one is dealing exclusively with heat in measuring dynamic heat capacity and that the imaginary parts of linear susceptibilities are normally related to dissipation.

To understand the meaning of the imaginary part of $C_p(\omega)$, perhaps it is profitable to consider more familiar dielectric susceptibility first. Suppose an oscillat-

ing electric field $E = E_0 \cos \omega t$ (real part of $e^{i\omega t}$; we use real, instead of complex, representation in this section) is applied to a dielectric sample with the dielectric susceptibility $\chi(\omega) = \chi'(\omega) - i\chi''(\omega)$. It is also supposed that the sample is in contact with the heat reservoir and the isothermal condition is maintained while the field is applied. Then the induced polarization is written as

$$P = \chi' E_0 \cos \omega t + \chi'' E_0 \sin \omega t \tag{16}$$

and the dissipation during one cycle is calculated to be

$$Q_{\text{diss}} = \oint \mathrm{d}t \frac{\partial P}{\partial t} E = \pi \chi'' E_0^2. \tag{17}$$

After one cycle of oscillation the sample goes back to its original state; what happens during the cycle is that the external field does work and this work is turned into heat Q_{diss}. It is of importance to realize that these processes occur in the sample, but the heat is transported to the reservoir to keep the sample temperature constant. Thus, the net result at the end of one cycle is the increase of entropy in the reservoir by an amount of

$$\Delta S_{\text{res}} = \frac{1}{T} \pi \chi'' E_0^2 \tag{18}$$

where T is the temperature of the sample. This result demonstrates that $\chi'' \geq 0$.

Now we move on to the dynamic heat capacity case. While the calorimeters we describe in this paper all adopt the second method of Section 2.3, it is heuristically easier to follow the first method in the discussion about the imaginary part. We suppose that the system temperature oscillates with $\delta T = \delta T_0 \cos \omega t$ since it is in contact with the reservoir whose temperature varies accordingly. Then the enthalpy of the system would vary as

$$\delta \langle H \rangle = C' \delta T_0 \cos \omega t + C'' \delta T_0 \sin \omega t \tag{19}$$

where C' and C'' denotes the real and imaginary parts of total heat capacity, respectively. Here again the system returns to its original state and nothing changes after one cycle; however, it can be easily seen that the entropy of the reservoir increases. To see this, note that the heat flow from the system to the reservoir is given by minus $\dot{Q}_{\text{fl}}$ where $\dot{Q}_{\text{fl}} = \mathrm{d}\delta\langle H \rangle / \mathrm{d}t$. Thus, the entropy change of the reservoir ΔS_{res} per one cycle is calculated to yield

$$\Delta S_{\text{res}} = \oint \mathrm{d}t \frac{-Q_{\text{fl}}}{T + \delta T} = \frac{1}{T} \oint \mathrm{d}t \dot{Q}_{\text{fl}} \left(-1 + \frac{\delta T}{T} \right)$$
$$= \pi C'' \left(\frac{\delta T_0}{T} \right)^2. \tag{20}$$

This result indicates that C'' leads to the entropy increase of the reservoir just as χ'' does and, of course, $C'' \geq 0$. Again it should be pointed out that the entropy production occurs *in* the sample as a result of the time lag of the system response during the heat exchange process.

3. Modulation calorimeters

3.1. Traditional ac calorimetry

Traditional ac calorimetry, initially developed by Kraftmakher [21] and Sullivan and Seidel [22], is a calorimetric technique in which a small amount of oscillating heat is supplied to a sample either by Joule heating or light heating and the ensuing temperature oscillation is measured. Since this temperature oscillation is inversely proportional to the heat capacity of the sample in the proper regime, one can determine the heat capacity of the sample by carrying out measurements at a judicially chosen frequency. While this method was mainly used to determine static heat capacity of materials [22–25], it is natural to attempt to extend the technique as a dynamic probe.

3.1.1. Energy balance equation

Consider a situation where an oscillating power is applied to a sample of typical thickness d. Suppose that the thermal diffusion time $\tau_D = d^2/D$, where D is thermal diffusivity, in a sample is very short compared to the period of an applied oscillating power. Or equivalently $d \ll \lambda$, where $\lambda = \sqrt{D/\omega}$ is the thermal wavelength. Thermal wavelength, naturally defined via the heat diffusion equation in Section 3.2.1, characterize the length over which the temperature oscil-

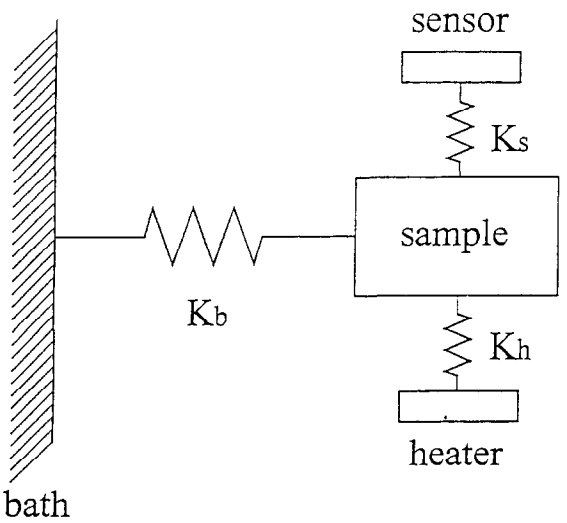

Fig. 3. Schematic diagram depicting a thermal situation of traditional ac calorimetry. A sample is connected to a sensor, a heater, and the bath by thermal conductances K_s, K_h, and K_b, respectively. It is usual that the sensor (thermocouple) and the heater (wire of 75 μm diameter) are very tightly attached to the sample and they have negligible heat capacities. Then the relaxation times related to K_s and K_h are very short and not to be considered. K_b is the only thermal conductance one needs to take into account.

lation decays. This can easily be achieved for a thin sample with high thermal conductivity by applying a sufficiently low-frequency power. Then, the sample may be regarded as oscillating in temperature as a whole without a temperature gradient and the situation can be dealt with using a simple energy balance equation [24]. Fig. 3 illustrates this situation of traditional ac calorimetry. A sample is connected to a sensor, a heater, and a surrounding shield (bath) by thermal conductances K_s, K_h, and K_b, respectively. However, provided that the sensor and the heater are very tightly attached to the sample and that they have negligible heat capacities, the relaxation times related to K_s and K_h are very short and can be neglected at frequencies of current interest, that is, below 1 Hz. (See the next section.) Thus, the only thermal link one has to consider is K_b and this may be due to the support lead connecting the sample to the shield, radiation, and/or residual gases.

Let $P_0 \exp(i2\omega t)$ be the ac power generated in the heater and $\delta\langle H\rangle$ be the enthalpy change of a sample assembly (sample+addenda) due to the ac power. (Here we use 2ω as the oscillating angular frequency of power, since we shall use the resistive heating as the power source. $f = \omega/2\pi$ is then the frequency of the electric current flowing through a heater and this is in accord with the convention of the 3ω technique in the next section. We shall often use f_T to denote temperature oscillating frequency, that is, $f_T = 2f$.) Then the energy balance equation is written as

$$P_0 e^{i2\omega t} = \frac{d\delta\langle H\rangle(t)}{dt} + K_b \delta T(t). \tag{21}$$

The first term of RHS of Eq. (21) represents the rate of heat absorbed by the sample assembly and the second term stands for the heat leak to the bath through the link. Since Eq. (21) is linear, the solution $\delta T(t)$ can be written as

$$\delta T(t) = \delta T^* e^{i2\omega t} \equiv |\delta T^*| e^{i\phi} e^{i2\omega t} \tag{22}$$

where δT^* is the complex amplitude of oscillation. Substituting Eq. (22) into Eq. (21), we have

$$P_0/\delta T^* = i2\omega C(2\omega) + K_b = i2\omega C' + 2\omega C'' + K_b \tag{23}$$

where C is the total heat capacity of the sample assembly. Equating the real and imaginary parts of Eq. (23) yields the following two equations for the temperature oscillation:

$$(P_0/|\delta T^*|)^2 = (2\omega C')^2 + (2\omega C'' + K_b)^2 \tag{24}$$

and

$$\phi = -\arctan\left(\frac{2\omega C'}{2\omega C'' + K_b}\right) \tag{25}$$

where $-\pi/2 < \phi < 0$. From these equations, C' and C'' can be written in terms of experimentally measured quantities $|\delta T^*|$ and ϕ as follows:

$$C' = -\frac{P_0}{2\omega|\delta T^*|}\sin\phi \tag{26}$$

$$C'' - \frac{P_0}{2\omega|\delta T^*|}\cos\phi - \frac{K_b}{2\omega} \tag{27}$$

Thus, if $C(2\omega)$ is indeed frequency dependent and has real and imaginary parts, one can obtain the dynamic heat capacity by measuring the magnitude and phase of δT^* as a function of frequency. In ordinary cases where the heat capacity is real, that is, $C'' = 0$, the magnitude and phase of the temperature oscillation become

$$|\delta T^*| = \frac{P_0}{\sqrt{(2\omega C)^2 + K_b^2}}; \quad \phi = -\arctan\left(\frac{2\omega C}{K_b}\right), \tag{28}$$

and K_b is given as

$$K_b = \frac{P_0}{|\delta T^*|}\cos\phi. \tag{29}$$

Before presenting experimental data, a couple of remarks are in order. First, we have neglected the effect of the dc power, P_0, which is always present in resistive heating in the above discussion. The dc power will simply raise the average temperature of the sample assembly with respect to the surrounding bath by an amount of $\Delta T = P_0/K_b$ and ac oscillation occurs around the raised temperature. This means that ac calorimetry does not operate in adiabatic environment and there exists a heat flow from the sample to the bath via K_b. Second, if K_b is chosen such that $K_b \ll \omega C$, then Eq. (28) becomes

$$|\delta T^*| \cong \frac{P_0}{2\omega C}, \quad \phi \cong -\pi/2 \tag{30}$$

and these are conditions for the quasiadiabatic regime where one normally works in the traditional ac calorimetry. The regime is called quasiadiabatic, since there is negligible ac heat loss during one cycle, although a dc heat flow is always present. Since we change frequencies in dynamic measurements, we are not necessarily in this regime and must take into account the effect of heat loss by using the full formula Eqs. (26) and (27).

3.1.2. Experimental results

In this section experimental data collected with the traditional ac calorimeter are presented after we briefly describe our experimental set-up. Fig. 4(a) shows the schematic diagram of the calorimeter. Surrounding a sample cell are a temperature controlled inner shield and a radiation shield. These shields are made of copper. The whole assembly is housed in a vacuum can (10^{-4} torr) and the can may either be immersed in liquid nitrogen or sit at room temperature. The inner shield is wound with a resistive wire and the temperature of the shield is controlled during operation using a commercial temperature controller or the PID temperature control program developed in this laboratory [26]. The instability of the temperature control is within 2 mK. We call the temperature controlled inner shield bath.

As for sample preparation, we directly attach a heater on a solid sample either by film deposition with a mask (see Fig. 12(b)) or winding a thin metallic wire. For a liquid sample, a cell is constructed usually with silver foils of typical thickness 0.1 mm; however, liquid CKN, our standard sample, turned out to interact even with noble metals. So aluminum was used for CKN cells. Since the upper frequency limit of the ac calorimetric method is set by internal diffusion time, the cell is made to have the thin rectangular cylindrical shape of approximate dimensions 10 mm × 1 mm × 10 *mm*. The schematic diagram of a typical cell is shown in Fig. 4(b). One can estimate the thermal diffusion time τ_D for the cell. For example, since the thermal diffusivity of CKN D is approximately 0.2 mm^2/s near the glass transition temperature [10], $\tau_D \simeq (d/2)^2/D$ of the cell is about 1.2 s. To further reduce τ_D by enhancing heat transport, we put pieces of aluminum wire in the cell. By following this preparation method, the highest frequency at which we obtained good data with CKN was about 0.13 Hz. The thick solid line vertically attached to the cell represents a copper lead of diameter 0.5 mm connected to the shield. The lead provided a mechanical support as well as a thermal link. (K_b is determined by this support lead for the most part and we shall come back to this point with experimental data.) Put on the top of the cell is a lid on which a sensor is attached. Temperature sensors used in the experiment with CKN were thermocouples. Thermocouples have negligible masses and consequently the thermal responses are instantaneous. Heater wire of diameter 75 μm is wound around the sample cell to yield ~30 Ω. Again the mass of heater wire is negligible.

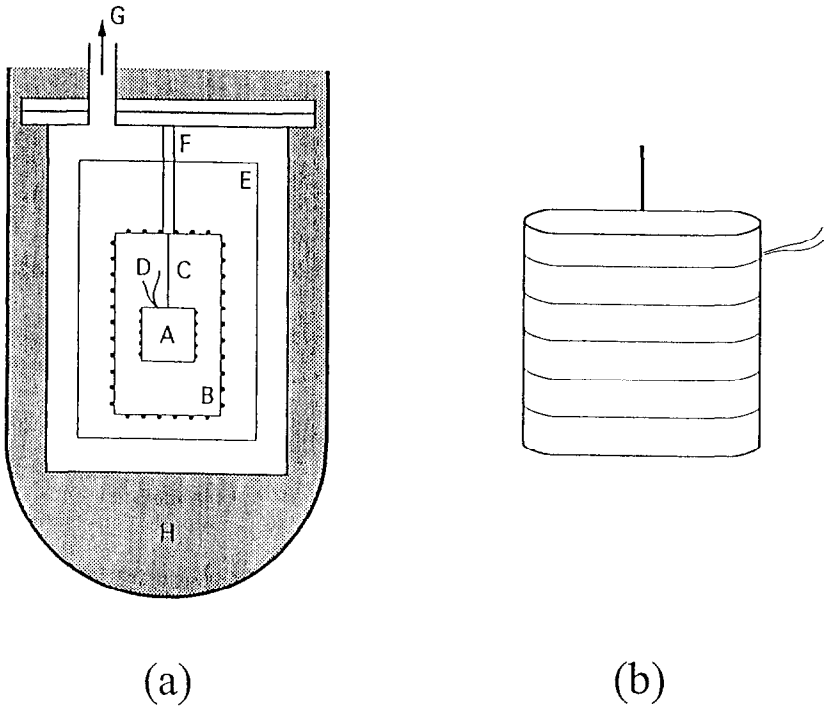

Fig. 4. Schematic diagrams of the traditional ac calorimeter, (a) the cryostat (b) a liquid sample cell: (A) sample assembly; (B) inner shield; (C) copper support lead; (D) temperature sensor; (E) radiation shield; (F) stainless steel tube; (G) vacuum line; (H) liquid nitrogen. The cell has the thin rectangular cylindrical shape of approximate dimensions 10 mm × 1 mm × 10 mm. The thick solid line vertically attached to the cell represents a copper lead (C) connected to the shield. The lead provides a mechanical support as well as a thermal link.

To induce temperature oscillation in the sample, the output from a frequency synthesizer is fed into the heater. The ensuing temperature oscillation (the magnitude is kept less than 20 mK, usually ~10 mK) in the sensor is measured with a digital nanovoltmeter triggered by the sync-out signal of the synthesizer and the signal voltage variations are read 64 points per period and 6 periods of temperature oscillation. To enhance precision, several data sets are averaged. To extract the magnitude and phase information, this averaged data set is fitted to the sinusoidal function with the quadratic background which compensates for the drift in temperature during data acquisition. The current supplied to the heater of the sample cell is separately calibrated to take into account the variation of the heater resistance as a function of temperature. All the electronic equipments are connected to a PC via IEEE-488 interface.

Before conducting an experiment with the ac calorimeter, one may check the characteristics of the calorimeter; this can be done in either the time domain or the frequency domain. The first method is to apply a constant amount of dc power, P_{dc}, to the sample. Then the temperatures of the sample and the shield are stabilized at T_0 and $T_0 - \Delta T$, respectively, where ΔT is given by P_{dc}/K_b. Now if the heater of the sample cell is turned off at $t = 0$, then the temperature of the sample, $T(t)$, will evolve exponentially, that is, for $\Delta T \ll T_0$,

$$T(t) = T_0 - \Delta T(1 - e^{-t/\tau_{link}}) \tag{31}$$

where

$$\tau_{link} = \frac{C}{K_b}. \tag{32}$$

From these measurements, one can obtain K_b and τ_{link}. Fig. 5 is the result for a particular sample cell filled with liquid CKN. After the cell was equilibrated at

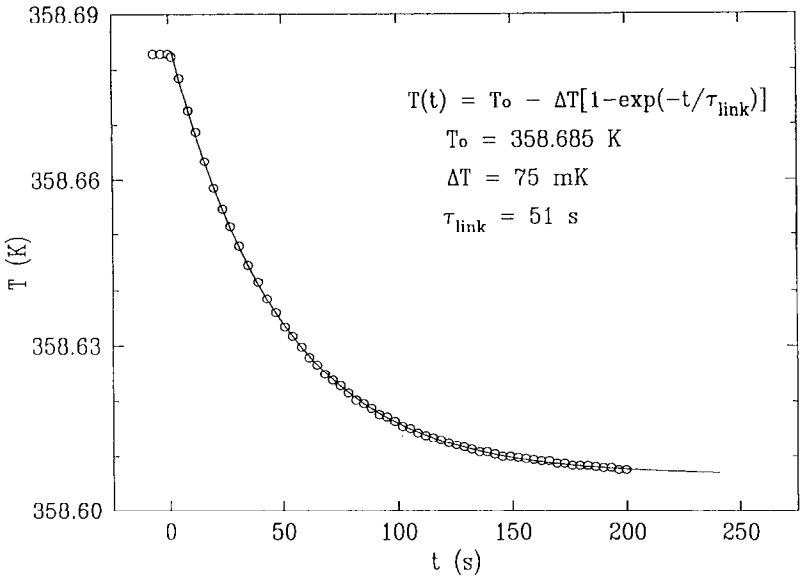

Fig. 5. Temperature relaxation data of the traditional ac calorimeter for liquid CKN at 358.6 K (circles): After the cell was equilibrated at T_0, 75 mK above the surrounding shield temperature, the heater was turned off. The solid line represents the fitting of the data to the exponential function of Eq. (31). The relaxation time τ_{link} so obtained is 51 s. Compare this result with that of the adiabatic calorimeter in Fig. 19.

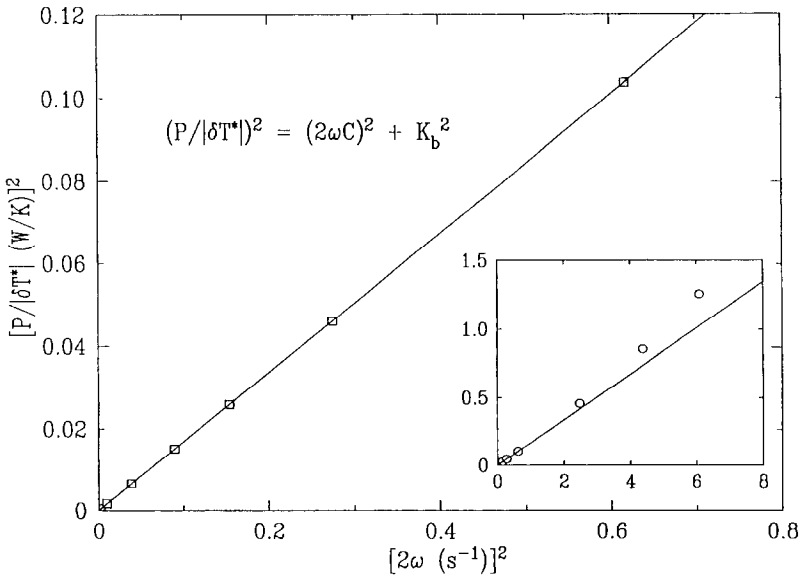

Fig. 6. Test of Eq. (24) of the liquid cell filled with CKN. Data points were taken at $T = 358.6$ K. Good linear relationship is found between $(P/|\delta T^*|)^2$ and $(2\omega)^2$ below $2\omega \approx 1\ s^{-1}$, that is, $f_T = 2f \approx 0.16$ Hz. Inset shows the deviation of the data points at high frequencies from the linear relationship due to the heat diffusion effects. From the slope C is found to be 0.41 J/K and the intercept value gives $K_b = 0.008$ W/K. This value of K_b is accounted for by heat conduction via the copper support lead.

$T_0 = 358.685$ K, $\Delta T = 75$ mK above the surrounding shield temperature, by applying $P_{dc} = 0.6$ mW, the heater was turned off. The solid line represents the fitting of the data to the exponential function of Eq. (31). The relaxation time τ_{link} so obtained is 51 s. From these values, we find that $C = 0.41$ J/K and $K_b = 0.008$ W/K.

The second test of the calorimeter is to check if Eq. (24) with $C'' = 0$ holds. Data points at various frequencies were taken at $T = 358.6$ K with the same CKN sample. As Fig. 6 shows, good linear relationship is indeed found between $(P/|\delta T^*|)^2$ and $(2\omega)^2$ below $2\omega \approx 1\,s^{-1}$, that is, $f_T = 2f \approx 0.16$ Hz. Inset demonstrates that the data points at high frequencies deviate from the linear relationship; this is probably due to the internal heat diffusion effects. From the slope C is found to be 0.41 J/K and the intercept value gives $K_b = 0.008$ W/K. These values are in good agreement with those obtained in the first method. It is noted that the value of K_b is accountable for the most part in terms of heat conduction via the copper support lead. Using the value of thermal conductivity of copper at 350 K, 3.96 W/cmK, length approximately 1 cm, diameter 0.5 mm, one finds that thermal conductance of the lead is approximately 0.0077 W/K. Thus, in our ac calorimetric set-up, heat conduction through the lead is larger than the heat leak due to radiation or gas conduction. It is pointed out that a reasonable value of K_b would produce small dc offset in ac calorimetry. (In adiabatic calorimetry, K_b is suppressed as much as possible to allow a large τ_{link}.)

Fig. 7 is the plot of the raw data of CKN, $P_0/2\omega|\delta T^*|$ and ϕ as a function of temperature measured by the traditional ac calorimeter. These data were taken at temperature oscillation frequency $f_T = 1/16$ Hz. While $P_0/2\omega|\delta T^*|$ shows the relaxational behavior, the phase varies unusually as temperature is reduced. Note that the phase has different values above and below the peak. This is the combined effect of the C' change and nonzero K_b in Eq. (25); of course, the peak in the phase is due to that of C''. In order to convert the raw data to C' and C'', it is necessary to run the separate experiment with the empty cell. This calibration run is done at a single frequency. From the data for the empty cell, one can obtain the heat capacity of the cell, C_{cell}, and K_b as a function of temperature using Eq. (26) and Eq. (29).

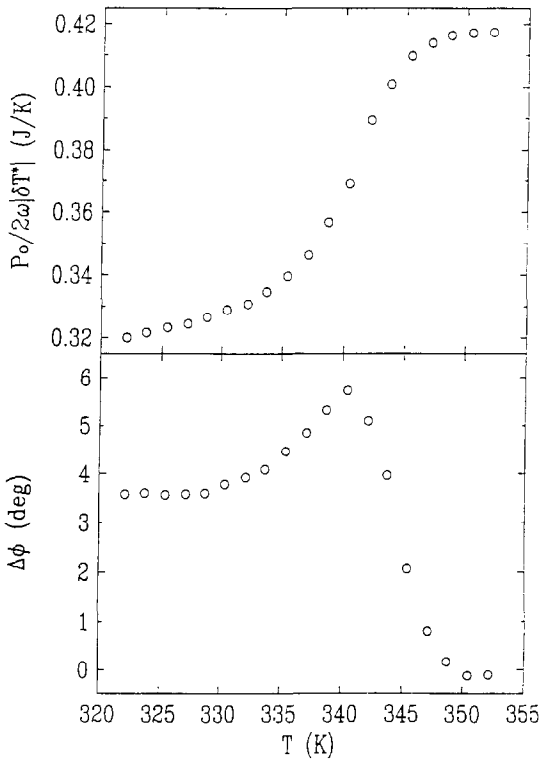

Fig. 7. Plot of $P_0/2\omega|\delta T^*|$ and the phase (raw data) of CKN as a function of temperature measured by the traditional ac calorimeter. The plotted phase values ($\Delta\phi$) are the relative change with respect to the high temperature value. Data were taken at temperature oscillation frequency $f_T = 2f = 1/16$ Hz. Note the unusual behavior of the phase variation as temperature is reduced; the phase has different values above and below the relaxation peak. After calibrating for the empty cell, these raw data are converted to dynamic heat capacity values.

Then the raw data is converted, using C_{cell} and K_b, according to Eqs. (26) and (27) to yield dynamic heat capacity values. Fig. 8 shows the dynamic heat capacity data of CKN at $f_T = 1/256$ and $1/8$ Hz. They show typical relaxational behaviors of a supercooled liquid. The transition from the high value of heat capacity to the low value occurs at different temperatures as the probing frequency is changed. However, since the dynamic range is limited ($0.0039 < f_T < 0.13$ Hz), one cannot cover the full spectrum of slow relaxation occurring in supercooled CKN with traditional ac calorimetry. Thus, we are content here with demonstrating that traditional ac calorimetry can

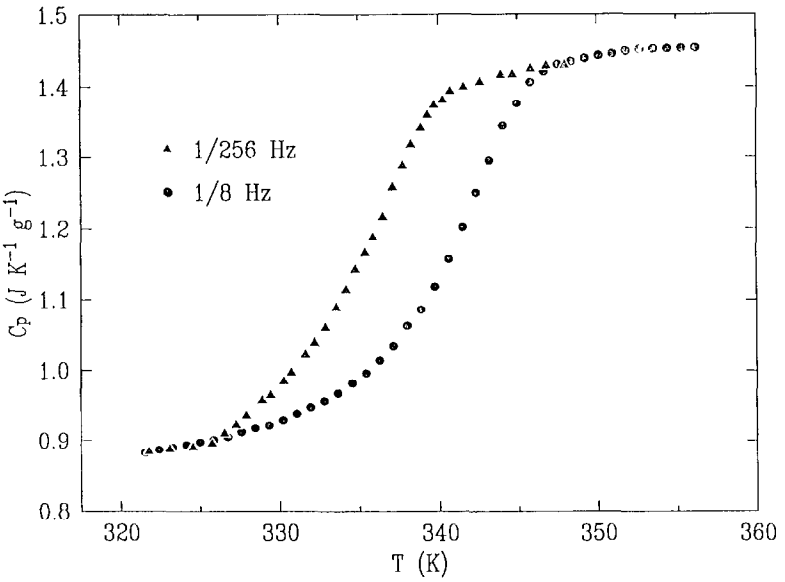

Fig. 8. The dynamic heat capacity data of CKN at $f_T = 1/256$ and $1/8$ Hz. They show typical relaxational behaviors of a supercooled liquid. Since the dynamic range is limited, one cannot cover the full spectrum with traditional ac calorimetry. This deficiency is overcome with the 3ω method.

indeed be used as a dynamic tool. The deficiency of limited dynamic range is overcome with the 3ω method. Even though ac calorimetry is not adequate to study glassy systems where response functions with very wide spectral width are ubiquitous, this method may have a role to play in investigations of biological systems if one can bring the upper frequency limit in liquid samples to a few Hz range with perhaps better designed sample cells [27]. Also by paying more attention to K_b one would be able to enhance the sensitivity at low frequencies.

3.2. The 3ω technique

In doing dynamic calorimetry with a traditional ac calorimeter, one tries to eliminate the effect of thermal conductivity and make a sample oscillating in temperature as a whole. One may add metallic wires for a liquid sample like CKN to enhance thermal conduction in the sample; for a solid sample, one may make it as thin as possible. However, there exists an unavoidable limit in this approach due to the fact that heat diffusion would produce a temperature gradient in the sample at high frequencies. Since the geometry of a sample here is not particularly well defined, it is very hard to deal with the situation where a temperature gradient exists in the sample. So the method is usually limited to less than 1 Hz for liquids or dielectric crystals and perhaps tens of Hz for metallic solids. To extend the dynamic range, one has to resort to a new method. A new method, the 3ω technique, we describe in this section takes advantage of a well-defined geometry with thickness of a sample much larger than the thermal wavelength to solve the heat diffusion equation and uses a heater as a sensor simultaneously to deal with the diffusive nature of heat. Since the sensor is at the same position as the heater (actually heater itself), we do not encounter a problem associated with the fact that the temperature oscillation decays within the thermal wavelength which becomes short at high frequencies. Thus, one can raise the upper limit of the dynamic range of modulation calorimetry. However, the price we pay for a large dynamic range is being involved with thermal conductivity.

Long ago Corbino [28] discovered that a third harmonic voltage, which is usually several orders of magnitude smaller than the fundamental, appears

when one applies an ac current to a resistive heater. Later on, Filipov and Rosenthal [29] used the bridge technique to measure the third harmonic signal. Since this third harmonic signal results from the temperature oscillation in the heater, Smith et al. exploited the method to measure frequency dependent heat capacity of germanium [6]. In 1985, Birge and Nagel [7] measured the dynamic heat capacity (actually heat capacity times thermal conductivity) of glycerol by using the third harmonic detection technique with planar heaters and showed the spectroscopic capability of this method. Cahill et al. [30] utilized a thin line heater to measure thermal conductivity of solids. Recently, we have demonstrated how to use heaters of arbitrary widths in the 3ω technique [31] and measured heat capacity and thermal conductivity of various liquid and solid samples [9,10,32]. Also Donth et al. have used the method to study the glass transition in various polymers [11].

3.2.1. Heat diffusion equation

Let us suppose that an infinitely long heater with a width $2b$ is placed on the surface of a semi-infinite medium as shown in Fig. 9, and it generates an oscillating power per unit length, $P_0 \exp(i2\omega t)$. (Here also exists, due to the dc component of power, a constant shift of the sample temperature with respect to the bath temperature, but it only causes a dc shift.) Using the result for an infinitely thin heater due to Carslaw and Jaeger [33] and remembering that the heater of width $2b$ can be regarded as a superposition of such thin heaters located between $-b$ and b, we arrive at the expression for the complex amplitude of the temperature oscillation at the surface:

$$\delta T^*(x, y=0) = \frac{P_0}{\pi\kappa}\int_0^\infty \frac{\cos(kx)\sin(kb)}{kb(k^2+q^2)^{1/2}}\,\mathrm{d}k \quad (33)$$

where κ is the thermal conductivity and q is the complex thermal wavenumber defined as

$$q = \sqrt{\frac{i2\omega C_p}{\kappa}}. \quad (34)$$

It is noted here that the thermal oscillation decays exponentially in the y-direction with a characteristic length, defined by various authors as the diffusion length, $\lambda = |q|^{-1} = \sqrt{\kappa/2\omega C_p} = \sqrt{D/2\pi}/\sqrt{2f}$, in which D is the thermal diffusivity. Because we shall use the heater as a sensor simultaneously (see Section 3.2.2), we calculate the temperature variation of the heater itself, δT_h, by taking the average of Eq. (33) from $-b$ to b, that is,

$$\delta T_h = \left(\frac{1}{2b}\right)\int_{-b}^{b} \delta T^*(x, y=0)\,\mathrm{d}x = \frac{P_0}{\pi\kappa}\int_0^\infty \frac{\sin^2(kb)}{(kb)^2(k^2+q^2)^{1/2}}\,\mathrm{d}k. \quad (35)$$

Since the analytic expression of Eq. (35) is not known, one has to resort to the numerical calculation to find out the frequency dependence of δT_h. As an example we chose the medium to be window glass. Using the thermal diffusivity, $D = 0.3\,\mathrm{mm^2/s}$, typical for window glass, we obtain $\sqrt{D/2\pi} = 0.22\,\mathrm{mm\,s^{-1/2}}$, and $\lambda = 220/\sqrt{2f}\,\mu\mathrm{m}$ where f is given in Hz. Fig. 10 is the calculated results for the heater of width $2b = 440\,\mu\mathrm{m}$. (This width was chosen somewhat arbitrarily for the sake of calculation.) Fig. 10 shows that the magnitude $|\delta T_h|$ (in units of $P/\pi\kappa$) is for linearly proportional to log $2f$ below 0.01 Hz, that is, $\lambda > 10b$. On the other hand, when $\lambda < b/10$, $\log|\delta T_h|$ is proportional to log $2f$ with the slope of $-1/2$ as is illustrated in Fig. 10(b). Fig. 10(c) displays the phase as a function of frequency. It should be noted that the phase has a constant value of -45 degrees at high frequencies.

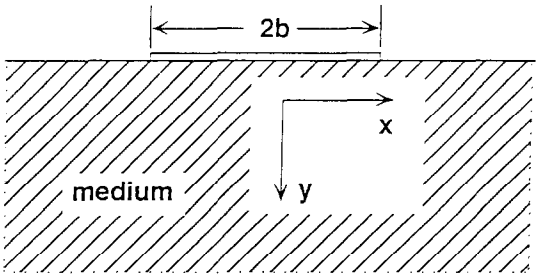

Fig. 9. Geometry of the heater and the medium. The medium is considered semi-infinite, and the heater of width $2b$ is regarded as a superposition of infinitely thin line heaters located between $x = -b$ and b. The heater is assumed to have a negligible mass and consequently no effect on the temperature profile of the medium.

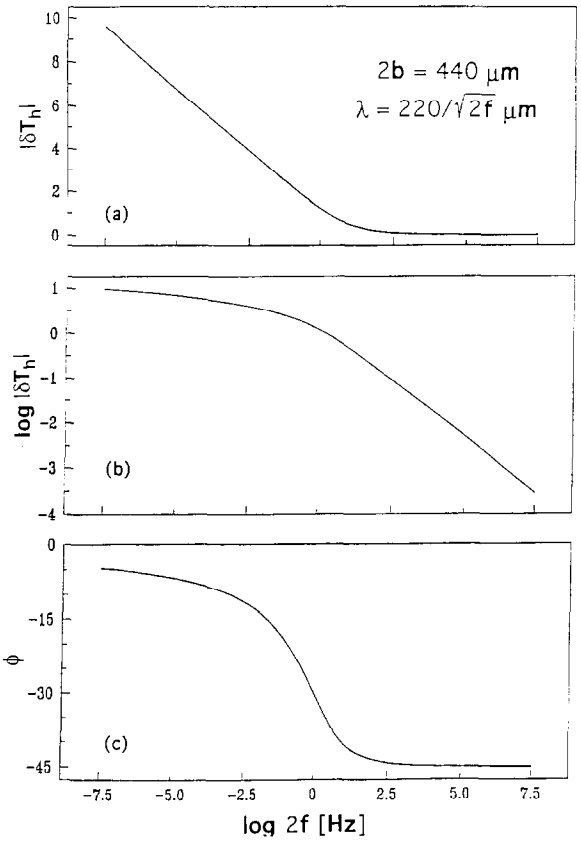

Fig. 10. The numerically calculated results for the heater of width $2b = 440\,\mu m$. The thermal decay length was taken to be $\lambda = 220/(2f)^{1/2}\,\mu m$ (f is in Hertz), which is a typical value for window glass. Magnitude $|\delta T_h|$ of the heater oscillation is given in units of $P/\pi\kappa$, while the phase is in degrees.

It is easy to see how these numerical results follow from Eq. (35). If $b \ll \lambda$, the integral can be carried out by first setting $\sin(kb)/(kb) = 1$. The result of integration is cast as

$$\delta T_h = \frac{P_0}{\pi\kappa}\left[-\ln\left(\frac{i2\omega b^2}{D}\right)^{1/2} + \eta\right] = -\frac{P_0}{2\pi\kappa}\ln 2\omega - \frac{P_0}{2\pi\kappa}\ln(b^2 C_p/\kappa) - i\frac{P_0}{4\kappa} + \frac{\eta P_0}{\pi\kappa} \tag{36}$$

where η is a constant having the value of $0.922\cdots$. Note that δT_h, more accurately its real part, $\mathrm{Re}[\delta T_h]$, is indeed linearly proportional to the logarithm of the measuring frequency. Since the coefficient of this linear term is inversely proportional to the thermal conductivity, one can obtain the thermal conductivity from the slope if one measures $\mathrm{Re}[\delta T_h]$ as a function of frequency in this regime. Thus, it offers a way to measure thermal conductivity of a medium with a relatively small temperature gradient by taking advantage of the well-established power of the ac modulation technique.

For the opposite case of $b \gg \lambda$, one can use a mathematical identity for the Dirac delta function [34]

$$\lim_{b\to\infty}\frac{1}{\pi b}\left[\frac{\sin bx}{\sin x}\right]^2 = \delta(x) \tag{37}$$

to obtain from Eq. (35)

$$\delta T_h = \frac{P_0/2b}{\kappa q} = \frac{P_0/2b}{\sqrt{2\omega C_p \kappa}}\,e^{-i\pi/4} \tag{38}$$

where $P_0/2b$ is now the power per unit area. (Or one can easily solve the one-dimensional heat diffusion problem to obtain the same result.) By working in this regime, one can measure the product of heat capacity and thermal conductivity, $C_p\kappa$, of the medium. Therefore, in principle by changing the measuring frequency to cover both regimes, one can obtain the thermal conductivity as well as the heat capacity of the medium separately. In addition, if the heat capacity becomes frequency-dependent, the magnitude and phase of δT_h would follow Eq. (38) with the complex, instead of real, $C_p(2\omega)$ as defined in Eq. (8). Thus the dynamic heat capacity can be obtained by measuring δT_h as a function of frequency.

When one deals with a liquid sample, one needs to evaporate a heater on a thick glass substrate. In this case the thickness of the substrate (like a solid sample) should be much greater than λ to avoid boundary effects from the back. A liquid sample is then put on top of the surface of the substrate. Now that there exist two different media on opposite sides of the heater, that is, a glass substrate and a liquid sample, we have to extend the previous results. For the planar heater, it is straightforward, since the symmetry of the boundary matches that of the one-dimensional heat diffusion, to

show that Eq. (38) becomes

$$\delta T_h = \frac{P_0/2b}{\sqrt{2\omega C_{pg}\kappa_g} + \sqrt{2\omega C_{pl}\kappa_l}} e^{-i\pi/4} \quad (39)$$

where the subscripts g and l stand for glass and liquid, respectively.

In case of a line heater, on the other hand, it may not be possible to solve the heat diffusion equation exactly. However, if we neglect the boundary mismatch [35], the problem can be written as a combination of two separate heat diffusions and, by defining $F(x) \equiv -\ln x + \eta$, δT_h is given as

$$\delta T_h = \frac{P_0}{\pi(\kappa_g + \kappa_l)} F(q_l b) \left[\frac{1}{1 + \frac{\kappa_g}{\kappa_l + \kappa_g}\left(\frac{F(q_l b)}{F(q_g b)} - 1\right)} \right] \quad (40)$$

where q_l and q_g denote the complex wavenumbers for the liquid and the glass, respectively. Since the quantity in the bracket Eq. (40) is very slowly varying with temperature, one can still obtain the sum of thermal conductivities from the slope of δT_h vs. $\log 2f$ (see Section 3.2.3). Thus, the glass contribution plays the role of background in both cases. To obtain the background information, one must carry out the measurements for the empty cell before taking data with samples. To implement above ideas into experimental reality, a method must be devised to detect the temperature variation of the heater itself. Also it becomes necessary to vary the width of the heater to cover the necessary range of b/λ, since the dynamic range needed to cover both regimes for a heater with a given width is far greater (14 decades) than is available experimentally.

3.2.2. Third harmonic detection

In order to measure the temperature oscillation of a heater itself we use the aforementioned third harmonic detection method, which is briefly described here. If one drives the heater with a current at frequency ω, $I(t) = I_0 \cos \omega t$, then one gets Joule heating at frequency 2ω at the heater and thus the temperature of the heater oscillates at the same frequency with the complex amplitude δT_h as given in the previous section. Since the heater is made of a metal such as gold or silver, its temperature coefficient of resistivity, $\alpha \equiv (1/R)(dR/dT)$, is not zero and as a result its resistance also oscillates at frequency 2ω. Thus,

$$R(t) = R_0[1 + \alpha|\delta T_h|\cos(2\omega t + \phi)] \quad (41)$$

where ϕ represents the phase shift of δT_h with respect to the power oscillation.

Due to the driving current $I(t)$ through the heater, the voltage across the heater appears as

$$\begin{aligned} V(t) &= I(t)R(t) = I_0 \cos \omega t \\ &\quad \cdot R_0[1 + \alpha|\delta T_h|\cos(2\omega t + \phi)] \\ &= I_0 R_0 \cos \omega t + \frac{1}{2} I_0 R_0 \alpha |\delta T_h| \cos(\omega t + \phi) \\ &\quad + \frac{1}{2} I_0 R_0 \alpha |\delta T_h| \cos(3\omega t + \phi). \end{aligned} \quad (42)$$

It is the second and third terms that contain the thermal information of the sample we want to measure. Note that they are relatively small compared to the first term since $\alpha \approx 0.004\ K^{-1}$ and $|\delta T_h|$ is usually kept less than 20 mK to stay in the linear regime. However, the last term, while small, appears at the third harmonic of the driving frequency and one can take advantage of this fact to measure the magnitude and the phase of the small signal in the presence of much larger unwanted signal using the Wheatstone bridge. The actual experimental set-up, which makes use of the Wheatstone bridge operated with a frequency synthesizer, is shown in Fig. 11. We refer other technical details to Ref. [9].

3.2.3. Experimental results

Since the frequency range available with the third harmonic detection scheme is limited generally from 0.01 Hz to 5 kHz, one has to vary the width of the heater to bring the experimental frequency window into the proper regime. (The upper limit comes from the requirement that the common mode rejection ratio of the differential preamplifier be greater than 120 dB due to the small 3ω signal level, while the low-frequency limit is given by the maximum time one can wait at a given condition.) The heaters with varying widths are obtained by thermally evaporating either gold or silver onto the polished surfaces of samples or substrates (for a liquid) through the masks whose patterns are shown in Fig. 12. The typical thickness of a heater is $\sim$1000 Å. This thickness is dictated by the conditions that the heater must be thin enough to be $\ll \lambda$ (otherwise one would be measuring the heater properties) and to disturb the temperature

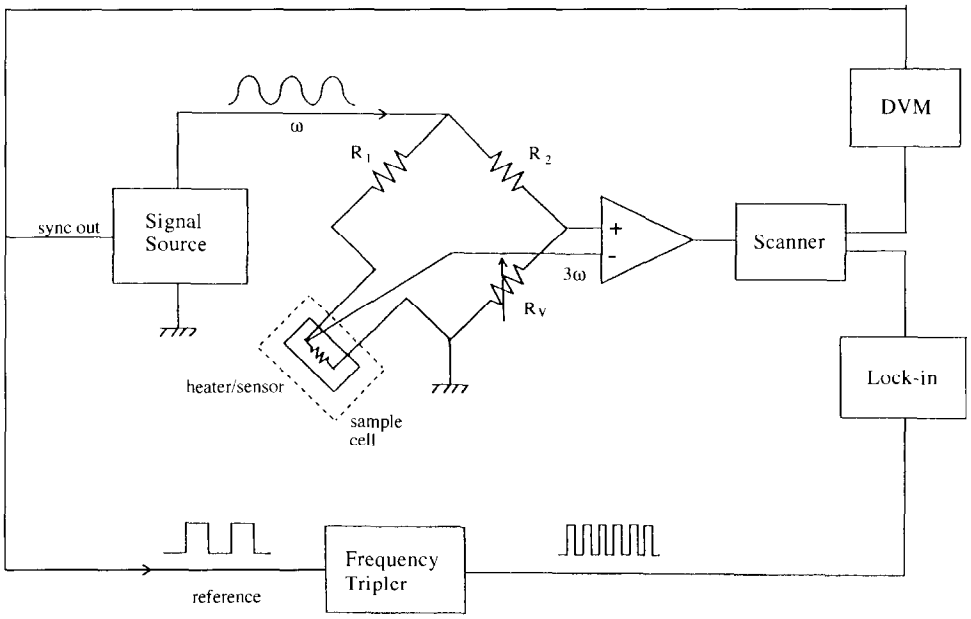

Fig. 11. Schematic diagram of the measuring circuit adopting the Wheatstone bridge. R_1 is a manganin wire with small temperature-coefficient of resistivity, and the resistances of R_2 and R_v are a few orders of magnitude larger than those of the left-arm resistances of the bridge. The scanner toggles the signal between the digital voltmeter (DVM) and the lock-in amplifier for below and above 1 Hz measurements respectively. Note that the three-probe method is used to remove the lead effects in balancing the bridge.

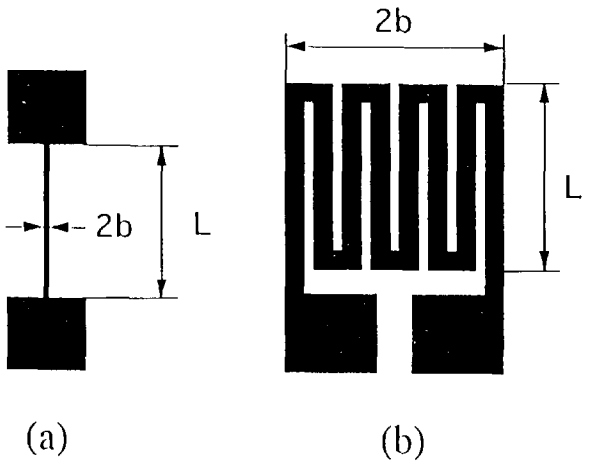

Fig. 12. The mask patterns used to produce line (a) and planar (b) heaters. The length (L) of the line heater is ~6 mm, while the width varies ($2b$). As for the plane heater, the line thickness, the total width ($2b$), and the length (L) are ~400 μm, 4 mm, 6 mm, respectively.

profile in the sample as little as possible. The length of line heaters is typically ~6 mm, while the width is varied down to 12 μm. In the case of plane heaters, we use the zigzag pattern as shown in Fig. 12(b) to obtain a reasonable value of resistance. Both the length of a heater and the thickness of a sample are required to be much greater than λ to satisfy the boundary condition assumed in solving the heat diffusion equation. The hardware arrangement surrounding the sample for the 3ω technique is nearly identical to that for the traditional ac calorimeter in Fig. 4(a).

To test the validity of the method, we made several samples of thick window glass (thickness = 1 cm $\gg \lambda$) deposited with heaters of varying width and checked if Eq. (35) was obeyed as a function of frequency. Measurements were done in the neighborhood of room temperature. To obtain the magnitude of δT_h, which is necessary to calculate C_p and κ, from the measured voltage signal, the knowledge of α in Eq. (42) is required. In the 3ω method, the resistance of the heater is automatically obtained in the course of the experiment, since the bridge is balanced at each temperature, and this allows one to calculate α. Fig. 13(a) and (b) show the magnitude of δT_h vs. logarithm of measuring frequency on linear and logarithmic scales for the glass samples with heaters of

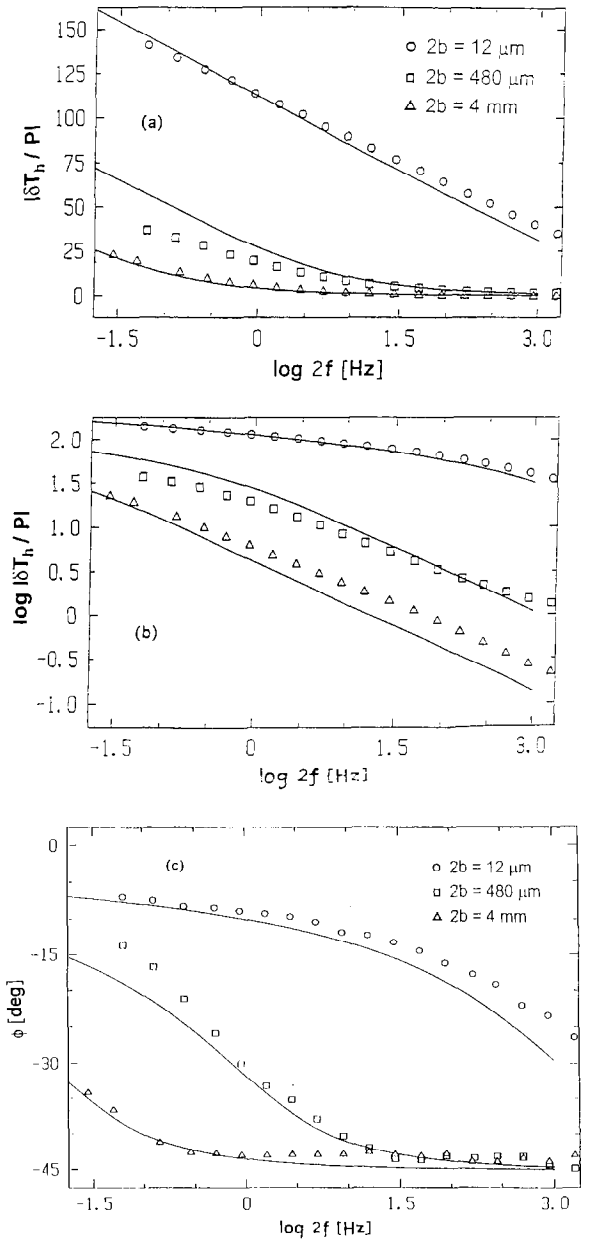

Fig. 13. Amplitude of temperature oscillation, δT_h, of the heaters of various widths on thick window glass vs. the logarithm of measuring frequency $2f$: (a) $|\delta T_h/P|$ vs. $\log 2f$; (b) logarithm of $|\delta T_h/P|$ vs. $\log 2f$; (c) the absolute phase of δT_h vs. $\log 2f$. The widths ($= 2b$) of the heaters are indicated in the figure. In (a) and (b), $|\delta T_h/P|$ (in units mK and mW, respectively) is plotted since the power level was changed as the measuring frequency varied.

various width. The lines in the figure were generated numerically from Eq. (35) using the known values of C_p and κ of glass. It is obvious from the figure that the agreement between the experimental data and the calculated values are fairly good for all cases. Especially encouraging is the obedience of the data to Eq. (36) and Eq. (38) in the two extreme regimes ($2b = 12\,\mu m$ and 4 mm) as can be seen in Fig. 13(a) and (b), since one would be largely working in these regimes where the interpretation of data is simple. When the width of the heater is in the middle, the crossover is seen as is predicted from Eq. (35).

To further confirm this obedience we have measured the absolute phase of the 3ω signal. This was done by calibrating the phase shifts of measuring circuits such as the preamplifier, lock-in amplifier, and the frequency tripler for the high-frequency measurements. Only the calibration of the preamplifier shift was necessary for the low-frequency data taken digitally with a digital voltmeter. The phase data and calculated values are compared in Fig. 13(c). Here again the agreement is excellent. Thus, these measurements provide the justification for the assumptions we made previously. For example, we assumed that the metallic heater on top of the sample would not affect the temperature profile in the sample. Also neglected was the fact that the length of the heater is finite instead of infinite as assumed. Now one can be fairly confident about the capability of the 3ω method as a tool for the measurement of thermal properties of a solid. Also we have shown that, even if the two extreme regimes give rise to simple interpretation of data, it is still possible to deal with the finite-size effects utilizing the general expression, Eq. (35).

The 3ω method was used to measure the thermal conductivity and the dynamic heat capacity in the supercooled state of CKN. Since the sample is liquid, we evaporated a heater on a glass substrate and put a short silica glass tube with the diameter slightly larger than the size of the heater as shown in the inset of Fig. 14. A small amount of CKN was put into the tube and melted. Fig. 14 displays the thermal conductivity data of the empty sample cell and CKN as a function of temperature. They were obtained from the slope of $\mathrm{Re}[\delta T_h]$ against $\log 2f$ for the empty and liquid-filled cell with a line heater of width $60\,\mu m$ according to Eq. (36) and Eq. (40). While κ_{cell} shows a linear behavior in temperature, κ_{CKN} displays a peculiar

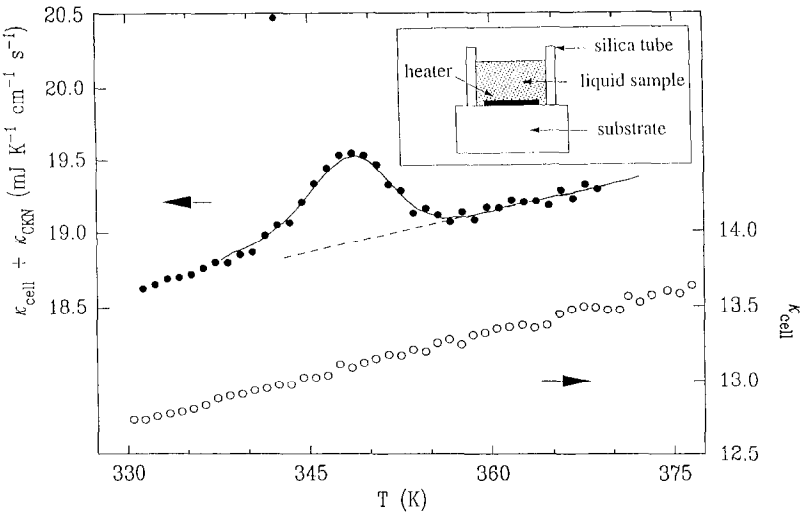

Fig. 14. Thermal conductivity of the cell, κ_{cell}, and the total conductivity, $\kappa_{cell} + \kappa_{CKN}$, obtained from the slope of $\mathrm{Re}[\delta T_h]$ of the line heater against $\log 2f$ are plotted as a function of temperature. The peak in $\kappa_{cell} + \kappa_{CKN}$ is solely due to the frequency-dependence of C_p of CKN, while the linear part is due to the cell contribution. The solid line represents the calculated values assuming that the thermal conductivity of CKN, κ_{CKN}, is constant. (See text.) Thus, κ_{CKN} is essentially constant and the true total conductivity is indicated by the broken line. Inset shows the liquid sample cell.

peak around 350 K. This behavior can be understood if we take into consideration the frequency dependence of C_p of CKN. When C_p is a frequency independent, real quantity at high and low temperatures, the term in the bracket of Eq. (40) shows little frequency dependence and its effect on the coefficient of $\log 2f$ is negligible (~0.05%). Thus, the slope gives rise to correct, total thermal conductivity of the cell and the sample. However, when C_p of CKN becomes frequency dependent, the coefficient of $\log 2f$ obtained from the blind linear fitting of the δT_h data yields an erroneous value for the thermal conductivity and one has to use the full expression of Eq. (40). In other words, the frequency dependence of C_p, which in turn makes the term in the bracket of Eq. (40) frequency dependent, does not allow the simple interpretation. If one insists on the linear relationship between $\mathrm{Re}[\delta T_h]$ and $\log 2f$, then the coefficient is no longer inversely proportional to thermal conductivity. To account quantitatively for the peak around 350 K, we calculated $\mathrm{Re}[\delta T_h]$, as a function of frequency, according to Eq. (40) by assuming κ of CKN is constant and using the $C_p(2\omega)$ values of CKN in Fig. 15. Then we obtained the coefficient of $\log 2f$ by linear fitting the calculated $\mathrm{Re}[\delta T_h]$ values against $\log 2f$. The solid line of Fig. 14 represents the results and it is in full agreement with the data. This fact clearly demonstrates that κ of CKN is essentially temperature independent [36].

Fig. 15 shows the dynamic specific heat capacity, $C_p(2\omega)$, of CKN measured by the 3ω technique as a function of temperature at various frequencies. (The values of frequency denoted in the figure are those of $f_T = 2f$.) These values of $C_p(2\omega)$ were obtained by dividing the planar heater data, $C_p(2\omega)\kappa$, with the constant value of κ of CKN from Fig. 14. $C_p(2\omega)$ shows a typical relaxation behavior of a supercooled liquid as is often seen in dielectric measurements. In other words, the real part shows dispersion and the imaginary part a peak as a result of the characteristic time of the system matching the probing time (=inverse frequency). In Fig. 16 shown are the real (C_p') and imaginary parts (C_p'') of the dynamic specific heat capacity of CKN vs. $\log f_T$. This figure clearly demonstrates that the 3ω technique offers dynamic range wide enough to cover the full response function. As is easily seen from the data, the dynamics of the system slows down with decreasing temperature (T) and the shape of C_p'' is asymmetrical. These features are typical of many glass formers; since it has been

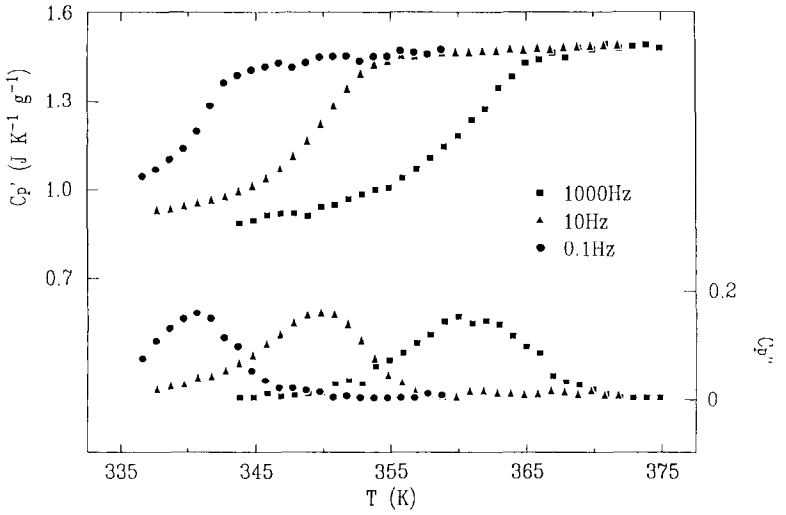

Fig. 15. Real and imaginary parts of the dynamic specific heat capacity of CKN at various frequencies are displayed as a function of temperature. The frequencies indicated in the figure are those of the temperature oscillation, f_T. The frequency dependent behaviors of C_p of CKN are those seen in typical relaxations.

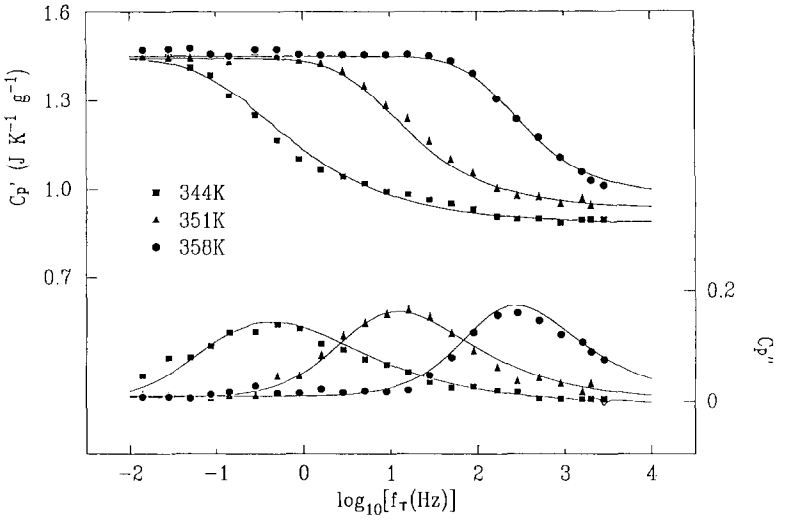

Fig. 16. The real and imaginary parts of frequency dependent heat capacity of CKN as a function of frequency, f_T. The solid lines are fits to the data with a Kohlrausch–Williams–Watts function, $\exp[-(t/\tau)^{\beta}]$, with $\beta = 0.53$ (344 K), 0.57 (351 K), and 0.62 (358 K).

found that the KWW (Kohlrausch–Williams–Watts) function adequately describes the dynamics for them, the data at each temperature were fitted with $R(t) = \exp[-(t/\tau)^{\beta}]$. To enhance the precision we have used the set of real and imaginary data simultaneously in fitting. The relaxation time $\tau = 1/2\pi f_T$ of CKN obtained with the modulation calorimeters (both the traditional one and the 3ω one) is shown against $1/T$, at which the peak occurs, in Fig. 17. The data illustrate that τ is not behaving in an Arrhenius

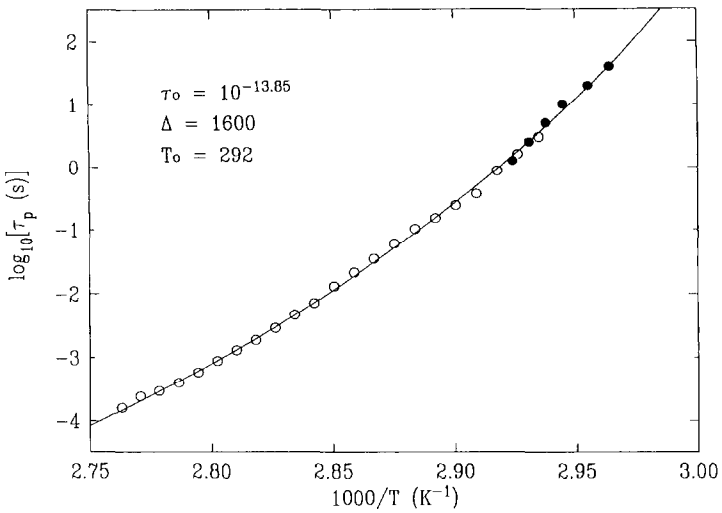

Fig. 17. The relaxation time of CKN, on a log scale, vs. T^{-1}. Plotted is the peak relaxation time, not average time. The open circles denote the relaxation time from the 3ω method, while the solid circles do those from traditional ac calorimetry. The solid line displays the Vogel–Fulcher fit, $\tau = \tau_0 \exp[\Delta/(T - T_0)]$.

fashion, but in a Vogel–Fulcher one. The solid line represents the best fit to the data using the Vogel–Fulcher form, $\tau = \tau_0 \exp[\Delta/(T - T_0)]$. The fitting procedure yielded the parameter values which are physically reasonable: $\tau_0 = 10^{-13.8}$ s, $\Delta = 1600$ K, $T_0 = 292 \pm 8$ K. Our combined data covers nearly 6 decades in frequency and represent the widest-frequency dynamic characterization of CKN to date.

3.3. Merits and demerits of modulation calorimeters

Modulation calorimetry, where one supplies a small oscillating heat input to a sample, allows one to measure the dynamic heat capacity in addition to the usual static heat capacity under equilibrium conditions. One can measure dynamic heat capacity directly with a traditional ac calorimeter. However, the dynamic range provided by this method is quite limited, below 1 Hz in many cases with solids as well as liquids. To extend the dynamic range, one can use the 3ω method. While this method raises the upper frequency limit to several kHz, one has to pay the price of being involved with thermal conductivity. To get dynamic heat capacity data, one has to perform separate measurements for thermal conductivity. It is also of value to point out that while the ac method gives high relative precision (up to a few part in 10^4 in a favorable situation), it is less accurate (probably a few %) in measuring the absolute value of heat capacity due to uncontrolled heat leak, radiation loss, etc.. Moreover, it is not possible to detect the latent heat associated with a first-order transition. Adiabatic calorimetry could be an alternative or supplementary method in this respect and this brings us to the discussion of adiabatic calorimeters.

4. Adiabatic calorimeters

4.1. Time domain dynamic calorimetry

One of the most difficult tasks in calorimetry is to contain leakage of heat, since there does not exist a perfect thermal insulator. Even if there were one, radiation would still have to be contained. In adiabatic calorimetry, heat leak from a sample to the surroundings is tightly controlled to zero. Since Nernst first constructed an adiabatic calorimeter [37], adiabatic calorimetry has been the most accurate method of determining static heat capacity. In this section we shall demonstrate that adiabatic calorimeters can also be used in measuring dynamic heat capacity. In using an adiabatic calorimeter for dynamic calorimetry, one is not aiming at extending the dynamic range. In fact,

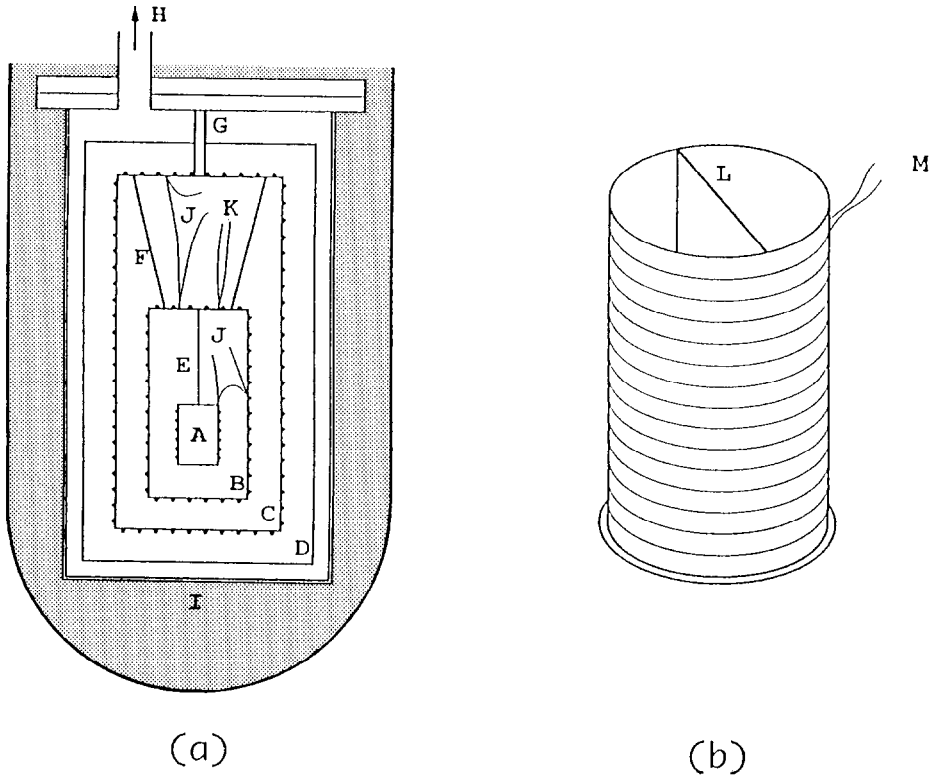

Fig. 18. Schematic diagrams of the modified adiabatic calorimeter, (a) the cryostat (b) a liquid sample cell: (A) sample cell; (B) inner adiabatic shield; (C) outer adiabatic shield; (D) radiation shield; (E) manganin wire; (F) stainless steel wire; (G) stainless steel tube; (H) vacuum line; (I) liquid nitrogen; (J) copper-constantan differential thermocouple, (K) *E*-type thermocouple, (L) partition of the cell, (M) manganin heater wire.

the size of the sample cell used in the adiabatic calorimeter is rather large compared to the one used in the traditional ac calorimeter. Even if one used a thin cell, one would still face the same high frequency or short time limit, set by internal heat diffusion, as in traditional ac calorimetry. The real virtue of adiabatic calorimetry as dynamic calorimetry lies in its ability to follow the slow relaxation in real time [38].

4.1.1. Hardware

We first briefly describe the hardware aspects of our adiabatic calorimeter set-up in this section. Fig. 18(a) shows the schematic diagram of the calorimeter. General arrangements for an adiabatic calorimeter are similar to those for a traditional ac calorimeter. However, there are a couple of important differences: In constructing an adiabatic calorimeter, we surround a sample with three shields, two temperature-controlled adiabatic shields and one radiation shield, to contain heat leak. Also, the links between a sample and the inner adiabatic shield and between shields are kept minimal in adiabatic calorimetry. In particular, the link between a sample and the inner adiabatic shield is the most critical and reduced to the point where heat loss is due mostly to radiation; the reason is obvious. From our experience it can be stated that the multiple shields and a minimal link between the sample and the inner shield are necessary conditions for successful adiabatic calorimetry.

For a solid sample, a heater may be directly attached. A cell must be constructed for a liquid sample using metal foils with high reflectivity to reduce radiation loss. For the experiment with our standard sample, liquid CKN, an aluminum foil of

thickness 0.1 mm is used to make a cell, whose schematic drawing is shown in Fig. 18(b). Thin manganin heater wire of approximately 120 Ω is wound around the sample cell and a thin layer of low-temperature varnish is used to ensure thermal contact. An aluminum partition is inserted into the cell for uniformity of temperature in the sample. The diameter d, volume, and mass of the cell are 0.8 cm, 1.0 cm^3, and 0.54 g, respectively. The typical amount of CKN in the sample cell is about 1.8 g, which is large compared to that in the ac calorimeter cell. Since our goal in adiabatic calorimetry is not increasing the dynamic range, we use the larger amount here compared to ac calorimetry. The larger heat capacity of the sample assembly helps increase τ_{link}. When the cell is filled with CKN, the thermal diffusivity of CKN D is about 0.2 mm^2/s near the glass transition temperature [10] and the thermal diffusion time, $\tau_D \simeq (d/4)^2/D$, of the cell is about 20 s. To eliminate a temperature gradient in the sample during measurements, we put aluminum wires into the liquid sample to reduce the thermal diffusion time as we do in traditional ac calorimetry. It should be ensured that the experimental results are independent of the amount of inserted wires.

Attached to the inner and outer adiabatic shields, surrounding a sample cell, are manganin heaters for controlling temperatures with resistances of 30 and 60 Ω, respectively. The outer adiabatic shield is made of copper. A polished silver sheet with 0.25 mm thickness is used for the inner adiabatic shield, which is of a cylindrical shape with diameter 2.5 cm and length 5.5 m, to reduce radiative heat loss. The sample cell is suspended from the inner shield by manganin wire with 75 μm diameter, and the inner shield is connected to the outer shield with stainless steel wires with 0.2 mm. The outer shield is then connected to the radiation shield by a stainless tube. The whole assembly is housed in a vacuum can and the can may either be immersed in liquid nitrogen or may sit at room temperature.

A pair of copper–constantan–copper differential junctions read the temperature difference between the outer shield and the inner shield, and the difference between the inner shield and the sample cell. The diameter of the differential thermocouple wires is 25 μm. For the absolute temperature reading, an E-type thermocouple junction is attached on the surface of the inner shield. Thermovoltages are measured with the resolution of 10 nV using digital nanovoltmeters. Temperatures are calculated from the calibrated thermovoltage versus temperature table by cubic spline interpolation. The resolution of the temperature measurements is about 0.5 mK at 100 K and 0.2 mK at 400 K. We use a computer-controlled power supply with multiple outputs as the power source for the three heaters on the sample, the inner shield, and the outer shield. The current supplied to the heater of the sample cell is measured using a digital multimeter to accurately calculate the input power to the sample. The resolution of the power measurement is about 0.03%. All the electronic equipments are connected to a PC via IEEE-488 interface and the temperatures of the adiabatic shields are controlled during operation using the PID temperature control program developed in this laboratory [26]. The difference voltage between the sample cell and the inner shield is used to maintain the adiabatic condition between the sample and the inner shield by varying a current to a heater on the inner shield. The outer shield temperature is controlled to stay at about 1 K below the inner shield by varying the current to a heater on the outer shield. Most of the temperature difference existing between the vacuum can wall and the sample is taken up by the outer shield, and thus the inner shield (and of course the sample) can maintain an isothermal condition over the whole body without a temperature gradient. The instability of the temperature control is within ±1 mK.

4.1.2. Energy balance equation

In the experimental set-up described above, we suppose that the temperature gradient in the sample cell is negligible and the whole sample assembly is at a single temperature denoted by T. Then the energy balance equation for the sample assembly (A of Fig. 18(a)) can be written as

$$P_{\text{in}} = C\frac{\mathrm{d}T}{\mathrm{d}t} + \dot{Q}_{\text{loss}}, \tag{43}$$

where P_{in}, C, and $\dot{Q}_{\text{loss}}$ are the input power to the sample, the heat capacity of the sample assembly, and the rate of the heat loss, respectively. Here the heat capacity of thin wires attached to the sample, such as the heater leads, the thermocouple wires, and the suspending wires, is assumed to be negligible. Since the calorimeter is operated under vacuum, the heat capacity of residual gases is also neglected. This is the

same equation as Eq. (21), but we pay more careful attention to the loss term in adiabatic calorimetry. Since the heat loss is due to radiation, convection by residual gases, and heat conduction by wires, $\dot{Q}_{\text{loss}}$ can be expressed as

$$\dot{Q}_{\text{loss}} = \sigma\mathcal{F}(T^4 - T_{\text{IS}}^4) + K_{\text{g}}\Delta T + K_{\text{w}}\Delta T, \tag{44}$$

where σ is the Stefan–Boltzmann constant, $\mathcal{F}$ is the shape factor which is related to the geometry and the emissivities of the cell and inner shield, and T_{IS} is the temperature of the inner shield. K_{g} and K_{w} are the thermal conductances of residual gases and wires connecting the sample cell and the inner shield, respectively, and $\Delta T = T - T_{\text{IS}}$ is the temperature difference between the sample cell and the inner shield. These three terms can be easily estimated [39]. For our set-up, if the residual gas pressure is kept less than 10^{-4} torr, the heat loss is mainly due to radiation because the residual gas contribution is about 1% of the radiation loss at 100 K, and 0.1% at 400 K and the last term due to the wires is of the same order of magnitude as the contribution of residual gases. The containment of $\dot{Q}_{\text{loss}}$, the most critical part of adiabatic calorimetry, is achieved by using triple shields and making τ_{link} as long as possible. The large τ_{link}, given by

$$\tau_{\text{link}} = \frac{C}{4\sigma\mathcal{F}T^3 + K_{\text{g}} + K_{\text{w}}}, \tag{45}$$

would permit the temperature controller to achieve $\Delta T = 0$, before any heat leak occurs. By reducing K_{g} and K_{w}, τ_{link} can reach more than thousand seconds and it is possible under this condition to keep ΔT virtually zero at all times.

4.1.3. Experimental results

In this section, we present experimental data obtained with liquid CKN. In order to estimate τ_{link} we first display in Fig. 19, the relaxation of the temperature of the cell at 300 K. After T was equilibrated at 301 K which was one degree above the shield temperature, the sample cell heater was turned off at $t = 0$ and $T(t)$ was recorded. The value of τ_{link}, obtained by fitting the data to Eq. (31), is 1256 s which appears to be large enough to control the inner shield temperature T_{IS} in order to maintain $\Delta T = 0$ all the time. It is of value to note that τ_{link} of the adiabatic calorimeter, where heat loss is due to radiation transfer for the most part, is about 20 times longer than that of the traditional ac calorimeter. (See Section 3.1.2.) We have utilized this adiabatic

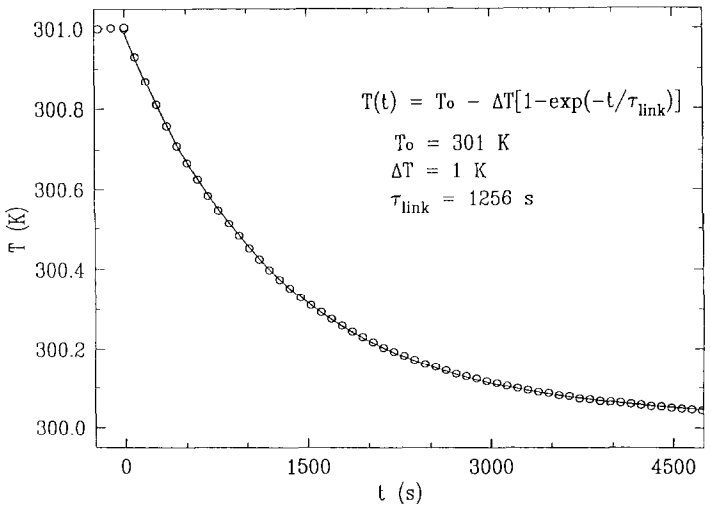

Fig. 19. Temperature relaxation data for the adiabatic calorimeter at 300 K (circles): The cell was filled with liquid CKN. After the cell was equilibrated at T_0, one degree above the shield temperature, the heater was turned off. The solid line represents the fitting of the data to the exponential function shown in the figure. The relaxation time τ_{link} so obtained is 1256 s.

calorimeter in measuring static heat capacity of ferroelectric crystals [40].

Now we wish to illustrate how we use the adiabatic calorimeter as a dynamic calorimeter in the time domain. Let us recall the situation depicted in Fig. 2(b). In time domain dynamic calorimetry, a certain amount of heat is applied instantaneously to a sample and its temperature response is examined in real time. By varying the values of applied energy, one can induce the temperature jumps of varying size. Fig. 20 illustrates, as an example, how the experiment of 1 K temperature jump is conducted. As is shown in Fig. 20(a), initially at $t = 0$ the pre-calculated amount of power (broken line), corresponding to 1 K increase in temperature, is applied to the inner shield for 10 s and then the power is turned off. It should be noted that the amount of power supplied to the inner shield under normal conditions ($t < 0$) is not zero. This is due to the fact that the inner shield is at 1 K above the temperature of the outer shield as stated above, and this fact is critical for the calorimeter to be capable of maintaining adiabatic conditions. At $t = 5$ s, the amount of power (solid line) needed to raise the sample temperature by 1 K is supplied for 5 s. The temperature variations of the sample (solid line) and the inner shield (broken line) caused by these power inputs are shown in Fig. 20(b). Between $t = 10$ s and the time at which the temperature of the shield overshoots as indicated by the thick arrows, the power input to the inner shield stays zero. But after this moment the temperature controlling action for the inner shield begins. The adiabatic status is achieved after the transient period of approximately 1 min elapses, as indicated in the figure by the light arrows.

While it is not easy to apply a large amount of power to a sample in modulation calorimetry, there is no difficulty in varying the temperature jump sizes in time domain dynamic calorimetry. This feature of the time domain method allows one to study nonlinear temperature relaxation. Thus, we investigated, using the adiabatic calorimeter, nonlinear temperature relaxation of supercooled CKN at $T_i = 328$ K. Initial temperature jumps of magnitude $\Delta T = 1, 2, 4$, and 8 K were induced by applying pre-calculated amounts of power to the cell and the inner shield in the same fashion as shown in Fig. 20. After the transient period elapses, the adiabatic relaxation, similar to that in Fig. 2(b), follows. The temperature relaxation of

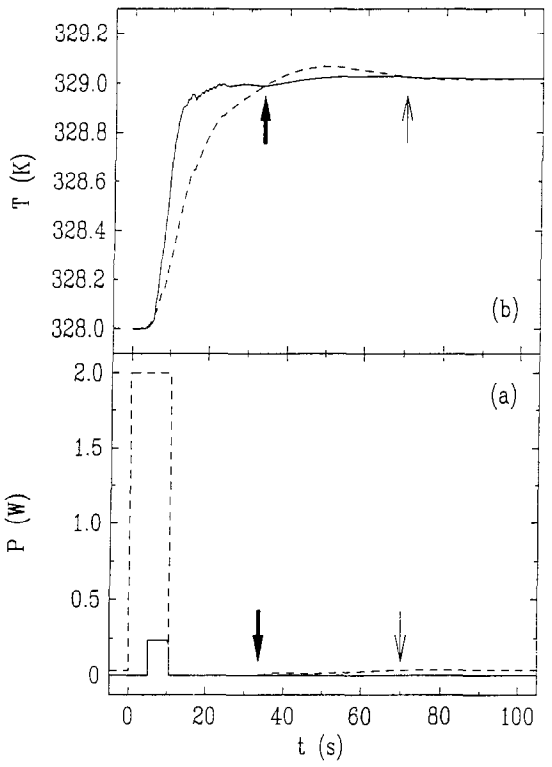

Fig. 20. In time domain dynamic calorimetry, a certain amount of power is applied to a sample and its temperature response is examined in real time. This figure illustrates, as an example, how the experiment of 1 K jump is carried out: (a) The pre-calculated amount of power (broken line), corresponding to 1 K increase in temperature, is applied at $t = 0$ to the inner shield for 10 s and then power is turned off. At $t = 5$ s, the amount of power (solid line) needed to raise the sample temperature by 1 K is supplied for 5 s. (b) The ensuing temperature variations of the sample (solid line) and the inner shield (broken line) are shown. When the temperature of the shield overshoots as indicated by the thick arrows, the temperature controlling action for the inner shield begins. The adiabatic condition is achieved (thin arrows) after the transient period of approximately 1 min elapses.

supercooled CKN manifests a strong nonlinear nature as displayed in Fig. 21. This behavior would have been difficult to study with any other method. The nonlinear nature of the relaxation can be accounted for by allowing β and τ of the KWW function, obtained for equilibrium situations, to vary in the course of relaxation. The lines in the figure was calculated in this way using the theory of Ref. [10]. Since the details of the calculations are very much involved, we only present the results [41].

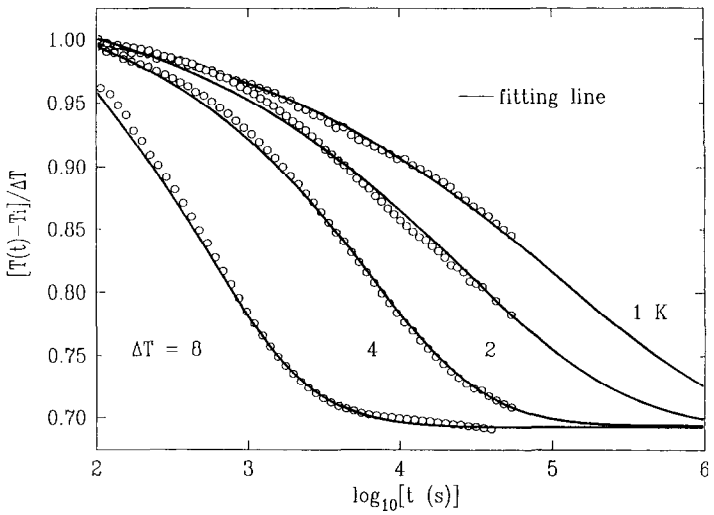

Fig. 21. Nonlinear temperature relaxation of CKN. Initially the system is at $T_i = 328$ K, and sudden temperature jumps of magnitude $\Delta T = 1, 2, 4$, and 8 K are induced by applying pre-calculated amounts of power to the cell and the inner shield as illustrated in Fig. 20. After the transient period elapses, the adiabatic relaxation of Fig. 2(b) follows. The nonlinear nature of the relaxation is accounted for, as indicated by solid lines, by using the theory of Ref. [10].

4.2. *Scanning modified adiabatic calorimeter*

One classical method to extract dynamic calorimetric information from a system is to perform scanning experiments [42]. In this method the experimental time scale is set by the scanning rate dT/dt. Commercial differential scanning calorimeters have been utilized for this purpose by other workers; however, a DSC generally does not yield accurate absolute values of heat capacity and even worse, it loses sensitivity at low scanning rates, in our experience below ~2 K/min. While the conventional adiabatic method allows operation in the scanning mode only in a heating experiment, it is necessary to measure heat capacity during cooling as well as heating at various scanning rates to extract dynamic information if a substance shows frequency dependence in heat capacity. This situation motivated us to develop a method to use an adiabatic calorimeter in a rate-scanning mode. The calorimeter used in this way is called *modified adiabatic calorimeter* (MAC) for the reason given in the next section and can be operated in both heating and cooling modes in the scanning range of 0.01–2 K/min. Thus, MAC is superb in probing extremely slow dynamic processes in condensed matter. MAC can also be operated as a scanning calorimeter for obtaining accurate values of static heat capacity in the heating or cooling mode.

4.2.1. *Controllable cooling rate of MAC*

The central idea of MAC is that $\dot{Q}_{\text{loss}}$ of Eq. (43) can serve as the cooling power if the inner shield is at a temperature lower than the sample [43]. Further, the value of $\dot{Q}_{\text{loss}}$ can be varied by changing the temperature difference between the sample and the shield. Note that at short times ($t \ll \tau_{\text{link}} \approx 20$ min), Eq. (31) becomes

$$T(t) = T_0 - \frac{\Delta T}{\tau_{\text{link}}} t. \tag{46}$$

Now if T_{IS} can always be maintained at $T(t) - \Delta T$ as $T(t)$ is changing, then continuous cooling is possible and the cooling rate is given by the following equation,

$$\frac{-dT}{dt} = \frac{\dot{Q}_{\text{loss}}}{C} \simeq \frac{4\sigma \mathcal{F} T^3 + K_{\text{g}} + K_{\text{w}}}{C} \Delta T. \tag{47}$$

Thus, it is possible to vary the cooling rate by varying ΔT, since T_{IS} can indeed be controlled in our set-up to be at $T(t) - \Delta T$ within ± 1 mK deviation at each instant during cooling. It is noted that since C and $\dot{Q}_{\text{loss}}$ does in general depend on T, it is difficult to keep the cooling rate precisely constant at all times.

Nevertheless, one can measure the heat capacity at reasonably different rates by using different values of ΔT.

The actual procedures for determining the heat capacity of a sample during cooling are as follows: one first fixes ΔT depending on the desired cooling rate. After T of the sample is equilibrated at ΔT above some initial temperature of the shield, one turns the sample heater off. As $T(t)$ decreases as a function of time, T_{IS} is continuously controlled to be at $T(t) - \Delta T$ and $T(t)$ is recorded. $\dot{Q}_{loss}$ is measured as a function of T and ΔT in separate experiments using the fact that $\dot{Q}_{loss}$ equals to P_{in}, which is directly measurable, in Eq. (43) when the system is in the steady state. ($\dot{Q}_{loss}$ may depend on T as well as ΔT, since the radiation term involves T^4.) Then the heat capacity C is calculated from Eq. (47) with the measured values of $T(t)$ and $\dot{Q}_{loss}$. For a given set-up $\dot{Q}_{loss}$ as a function of T and ΔT was reproducible as long as the residual gas pressure was kept less than 10^{-4} torr. In the heating measurement, as is usual with adiabatic calorimetry, T_{IS} is controlled to satisfy the adiabatic condition, while P_{in} is supplied to the heater of the sample cell. For $\Delta T \leq \pm 1$ mK, $\dot{Q}_{loss}$ is negligible and the heat capacity can be measured in the adiabatic condition by the heat pulse method or the continuous heating method.

4.2.2. Experimental results

Since it is essential for MAC to have a capability of varying the cooling rate to function as a dynamic calorimeter, we first show, in Fig. 22, that the linear relationship between the cooling rate and ΔT holds at 300 K as expected from Eq. (47). The inverse of the slope is 1232 s, which is consistent with the fact that τ_{link} is equal to the inverse of the slope from Eq. (45) and Eq. (47). The variable range of cooling rate from 0.01 to 2 K/min can be achieved by varying ΔT from 0.2 K to 40 K. In this range, it is difficult to measure the heat capacity using the conventional DSC because the resolution is degraded below 2 K/min.

Fig. 23 is a typical temperature versus time (T vs. t) trace as one cycle experiment to determine the heat capacity of CKN. The cooling and heating curves were obtained under the conditions of $\Delta T = 12.6$ K and $\Delta T = 0$ K, respectively. These conditions were satisfied at all times within ± 1 mK. The procedures for the cooling run are described in the previous section. In obtaining the heating data, we applied a constant amount of power, producing the same rate as the cooling rate, to the sample and controlled T_{IS} to meet the adiabatic condition as T increased. From the T vs. t curve, one can calculate the scanning rate dT/dt at each temperature using the Savitzky–Golay filtering algorithm [44] to reduce the short-term noise which is

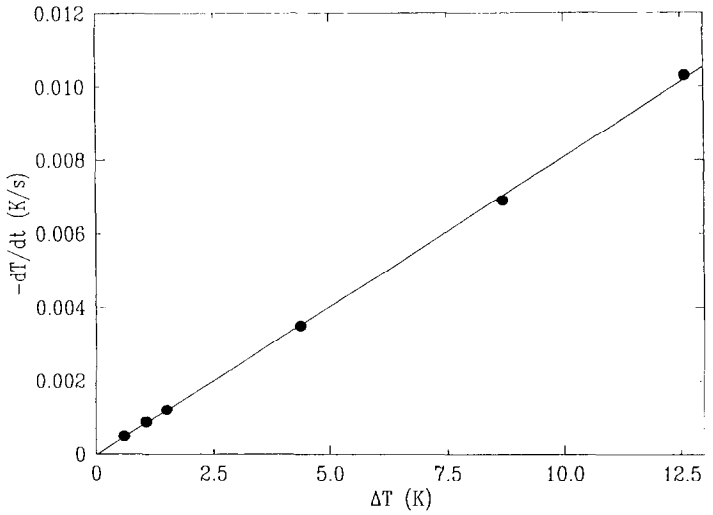

Fig. 22. The cooling rate ($-dT/dt$) as a function of ΔT at 300 K (filled circles): The solid line shows the linear relationship and the inverse of the slope (= 1232 s) should be equal to τ_{link} of Fig. 19.

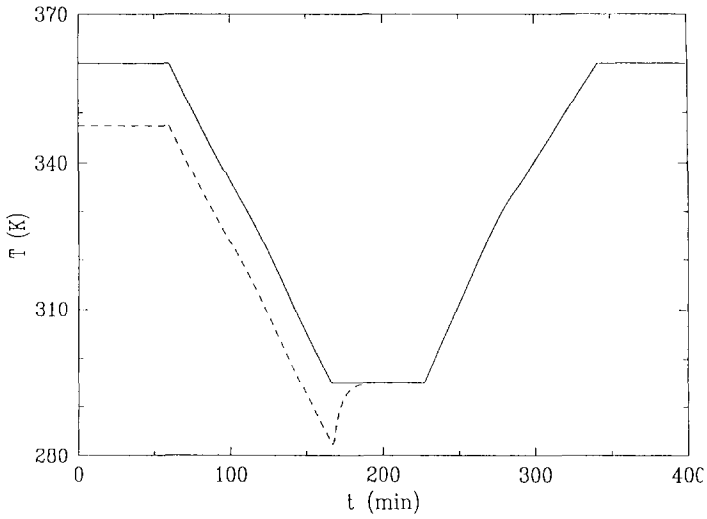

Fig. 23. A typical temperature vs. time curve obtained by MAC. During the cooling scan, there exists a constant difference between the temperature of the sample (solid line) and that of the shield (broken line), while they are the same in the heating scan.

due to the numerical differentiation. Fig. 24(a) shows the cooling rates calculated from the data obtained in the runs with $\Delta T = 1.5$ and 12.6 K. The average cooling rates for the whole temperature range are 0.07 and 0.6 K/min, respectively. $\dot{Q}_{\text{loss}}$ measured in three degree steps as a function of temperature in the above two cases is shown in Fig. 24(b). For intermediate temperatures, the data are fitted to a fourth-degree polynomial in T. From the data of Fig. 24(a) and Fig. 24(b), the heat capacity, $C = \dot{Q}_{\text{loss}}/[-\mathrm{d}T/\mathrm{d}t]$, was calculated and plotted in Fig. 24(c). In converting $T(t)$ on the heating side to the heat capacity, only $\mathrm{d}T/\mathrm{d}t$ is needed since the input power to the sample is constant. The final data of heat capacity of CKN are obtained after the contribution of the empty cell, measured in a separate run, is subtracted. In Fig. 25 we show the heat capacity data obtained from various methods such as DSC, modulation calorimeter, and MAC [10]. The values of heat capacity of the liquid and glass parts are in excellent agreement, while they show relaxational behaviors in the transition region. Therefore MAC extends the dynamic range of heat capacity measurements far below existing methods, in addition to providing the absolute values of heat capacity. The accuracy of MAC in this case is found to be within 0.35%.

In closing this section we wish to show that the heat capacity data of supercooled CKN one obtains with scanning calorimeters (either DSC or MAC) are fully accountable in terms of the frequency-dependent heat capacity data generated by modulation calorimeters. We should point out that the frequency dependent heat capacity is the equilibrium property of a system, because only a small oscillating heat is applied and one remains in the linear response regime throughout the measurements. On the other hand, the heat capacity data one obtains with scanning calorimeters are the results of the system falling out of equilibrium as the system temperature is reduced at a certain rate. (The converse is true in the heating case.) However, we have shown that this ergodic–nonergodic glass transition (falling out of equilibrium) is basically a phenomenon due to the splitting-off of the slow relaxing modes from the rest and the associated relaxation can be described in the theoretical framework for the equilibrium relaxation if the latter is properly modified [10]. The results are shown in Fig. 26. We refer the reader to Ref. [10,41] for details.

4.3. Merits and demerits of adiabatic calorimeters

An adiabatic calorimeter is the most accurate tool for heat capacity and latent heat measurements. In particular, the latent heat information is very hard to obtain by other methods. With the advance in computer control and electronics technology, the operation

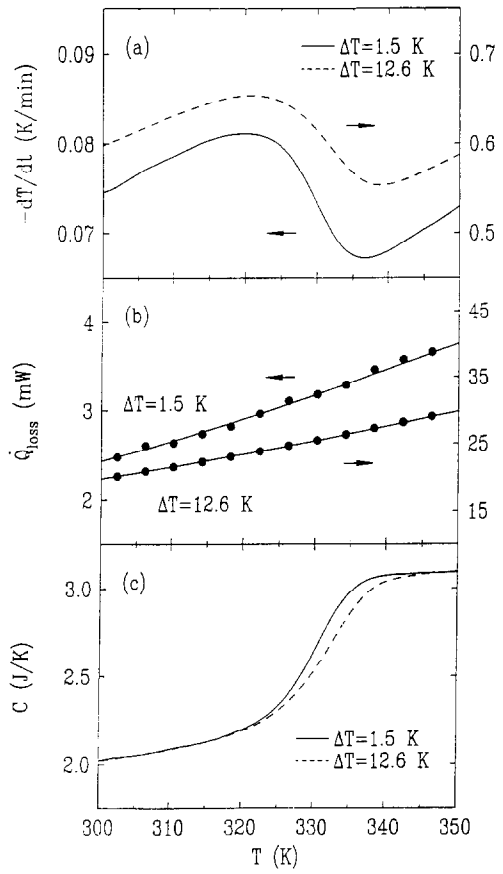

Fig. 24. (a) Calculated cooling rates of CKN for $\Delta T = 1.5$ and 12.6 K. (b) The measured values of heat loss, $\dot{Q}_{loss}$, is denoted by dots for $\Delta T = 1.5$ and 12.6 K and the lines represent the polynomial fitting. (c) Heat capacity of the sample assembly calculated from $-dT/dt$ and $\dot{Q}_{loss}$.

of adiabatic calorimeters has become less tedious and less time-consuming. This advance has allowed the time domain dynamic calorimetry where one follows, after a certain amount of heat is given to a system, the temperature change of the system under adiabatic conditions. Enthalpy relaxation, including nonlinear relaxation, can be studied in real time with adiabatic calorimeters. It was demonstrated that heat capacity measurements can be conducted at extremely low scanning rates with a modified adiabatic calorimeter. By combining modulation and adiabatic calorimetry, one can obtain dynamic as well as static calorimetric information about a given sample with accuracy and precision.

5. Summary and future outlooks

In this paper, we have reviewed dynamic calorimetric techniques currently in use in our laboratory. We have attempted to show that the temperature modulation method and the adiabatic method are complementary and applying these techniques to a physical system provides us more complete view of the physical phenomena occurring in the system. Each method was tested with the standard sample, CKN. To keep the point of the paper focused, we have refrained from presenting data obtained for diverse physical phenomena. However, it is recognized that dynamic calorimetry has wider applications. For example, biological systems, where slow dynamics is an often important occurrence, may be suitable to be studied by dynamic calorimetry. In fact, there already exist attempts in this direction [27] and our methods, which have a larger dynamic range than is used in the field, may be exploited beneficially. Also of keen interest and a good candidate where one can expect a contribution from dynamic calorimetry is the melting phenomenon. Here the latent heat and heat capacity effects are usually entangled in calorimetric measurements to make the interpretation of data obscure; however, by combining various methods presented here one can hope to disentangle them. Although solid samples were not discussed at all, one can also expect to find its usage in situations involving solids: global thermal hysteresis phenomenon in incommensurate ferroelectrics, heat conduction in porous media and so on.

In addition to applying the current techniques to various problems, the following areas may be pursued in the future research: One may try to extend the dynamic range of the 3ω method above the current frequency limit, a few kHz. If successful, then the thermal wavelength can enter the submicron regime in dielectric materials. This would allow the characterization of thermal properties of thin films with submicron thickness. This information is not only scientifically interesting (heat capacity and thermal conductivity of a sample with restricted geometry) but also technologically demanding (efficient heat transport in thin films). The development of noncontact heating at higher frequencies than is available with the present light chopping would be very helpful in enhancing the applicability of modulation

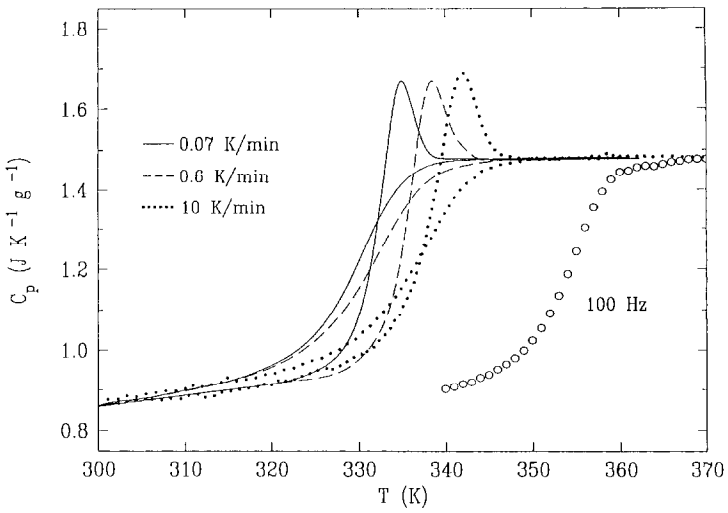

Fig. 25. Specific heat capacity of CKN measured by various methods. MAC data for continuous cooling and heating at the average rates of 0.07 K/min (solid line) and 0.6 K/min (broken line), DSC data at 10 K/min (dots), and dynamic heat capacity data at 100 Hz (circles) [10] are shown.

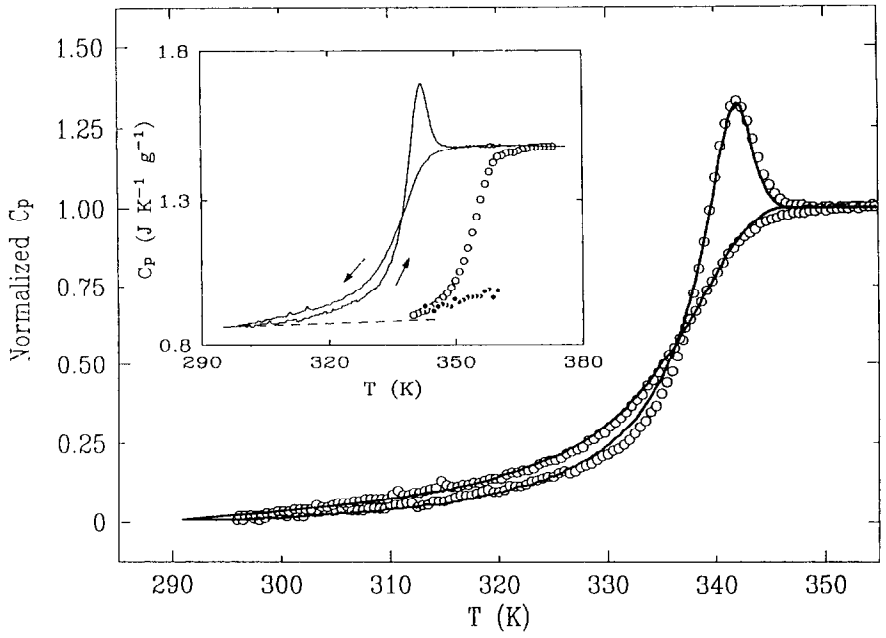

Fig. 26. This figure illustrates that the data obtained with a scanning calorimeter is accountable in terms of the response function yielded by modulation calorimeters. The open circles represent the normalized heat capacity of CKN, $[C_p(T) - C_{pg}(T)]/[C_{pl}(T_f) - C_{pg}(T_f)]$, and the solid lines are from the calculation presented in Ref. [10]. Here C_{pg} and C_{pl} denote the heat capacities of glass and liquid, respectively. T_f is the fictive temperature as introduced in Section 2.2. Inset shows the DSC data on cooling and heating at 10 K/min (solid lines) and the dynamic heat capacity data at 100 Hz (circles). The dots in the inset denote C_p^{∞} values of the equilibrium liquid, while the broken line does C_{pg}. For details, see Ref. [10].

calorimeters. Finally, we mention a very interesting possibility. Since we have generalized heat capacity temporally by defining dynamic heat capacity, one may also attempt to generalize heat capacity spatially by defining heat capacity which is wavenumber- as well as frequency-dependent [45]. This full generalization of heat capacity would constitute a challenge theoretically as well as experimentally.

Acknowledgements

Most of the work presented in this paper was done with the assistance of Mr. I.K. Moon and I am very much thankful to him for overcoming all the technical difficulties in developing dynamic calorimetry. Financial support by Korea Science and Engineering Foundation (941-0200-018-2), Excellence Science Research Center RCDAMP of Pusan National University, and Basic Science Research Institute program of Pohang University of Science and Technology (95-2438 and special fund) are gratefully acknowledged.

References

[1] A. Lavoisier, Elements of Chemistry, Paris, 1789.
[2] B. Wunderlich, Thermal analysis, Academic Press, San Diego, 1990.
[3] In this paper three kinds of heat capacity appear: an extensive variable, total heat capacity, and two intensive variables, heat capacity per unit volume and heat capacity per unit mass. We shall use the term *heat capacity* to mean heat capacity per unit volume in the theoretical discussion unless otherwise stated, since it appears naturally in the heat diffusion equation. On the other hand, experimental results are usually given in terms of specific heat capacity (heat capacity per gram). Following this convention, experimental data are presented in terms of specific heat capacity.
[4] K.F. Herzfeld and F.O. Rice, Phys. Rev., 31 (1928) 691.
[5] M. Fixman, J. Chem. Phys., 33 (1960) 1363; 36 (1962) 1961.
[6] R.C. Smith, J. Appl, Phys., 37 (1966) 4860; R.C. Smith and L.R. Holland, J. Appl. Phys., 37 (1966) 4866.
[7] N. Birge and S. Nagel, Phys. Rev. Lett., 54 (1985) 2674; Rev. Sci. Instrum., 58 (1987) 1464.
[8] P. Dixon and S. Nagel, Phys. Rev. Lett., 61 (1988) 341; P. Dixon, Phys. Rev., B42 (1990) 8179.
[9] D.H. Jung, T.W. Kwon, D.J. Bae, I.K. Moon and Y.H. Jeong, Meas. Sci. Technol., 3 (1992) 475.
[10] Y.H. Jeong and I.K. Moon, Phys. Rev., B52 (1995) 6381.
[11] Donth et al. in this issue.
[12] O. Nakada, J. Phys. Soc. Japan, 15 (1960) 2280.
[13] Of two assumptions, causality is naturally always satisfied while analyticity is not guaranteed to hold in every situation; nevertheless it seems that analyticity may be assumed to hold in most cases.
[14] R. Kubo, Rep. Prog. Phys., 29 (1966) 255.
[15] $\langle H \rangle$ here represent the ensemble average of $(\mathscr{H}_0 + pV)$ in statistical mechanics. The thermodynamic quantity H of Eq. (1) is equal to $\langle H \rangle$ here.
[16] We shall use the angular frequency ω and the frequency $f = \omega/2\pi$ interchangeably.
[17] One may use the opposite convention of time-varying factor $\exp(-i\omega t)$, then the dynamic heat capacity would be defined as $C_p(\omega) = C_p'(\omega) + iC_p''(\omega)$.
[18] A.B. Bhatia, Ultrasonic absorption, Dover Pub., New York, 1967, Chap. 5.
[19] C. Kittel, Introduction to Solid State Physics, John Wiley & Sons, New York, 1986.
[20] A. Q. Tool, J. Res. J. 34 (1945) 199; J. Am. Cer. Soc. 29(9) (1946) 240.
[21] Y.A. Kraftmakher, Zh. Prikl. Mekhan. i Tekhn. Fiz., 5 (1962) 176.
[22] P.F. Sullivan and G. Seidel, Phy. Rev., 173 (1968) 679.
[23] I. Hatta, Pure & Appl. Chem. 64 (1992) 79; See also I. Hatta in this issue.
[24] C.W. Garland, Thermochimica Acta 88 (1985) 127; K.J. Stine, Ph.D. thesis, Massachusetts Institute of Technology (1988).
[25] K. Nahm, C.K. Kim, M. Mittag and Y.H. Jeong, J. Appl. Phys., 78 (1995) 3980.
[26] T.W. Kwon, D.H. Jung, D.J. Bae and Y.H. Jeong, Kor. J. Appl. Phys., 4 (1991) 133.
[27] E. Freire, W.W. van Osdol, O.L. Mayorga and J.M. Sanchez-Ruiz, Annu. Rev. Biophys. Chem., 19 (1990) 159.
[28] O.M. Corbino, Phys. Z., 12 (1911) 292.
[29] L.P.Filipov, Inzh. Fiz. Zh., 3 (1960) 121; L.A. Rosenthal, Rev. Sci. Instrum., 32 (1961) 1033.
[30] D.G. Cahill, H. E. Fisher, T. Klitsner, E.T. Swartz and R.O. Pohl, J. Vac. Sci. Technol. A 7 (1989) 1259; D.G. Cahill, Rev. Sci. Instrum., 61 (1990) 802.
[31] I.K. Moon, Y.H. Jeong and S.I. Kwun, Rev. Sci. Instrum., 67 (1996) 29.
[32] Y. H. Jeong, D.J. Bae, T.W. Kwon, I.K. Moon, J. Appl. Phys. 70 (1991) 6166; D.J. Bae, K.B. Lee, Y.H. Jeong, S.M. Lee and S.I. Kwun, J. Kor. Phys. Soc. 26 (1993) 137; S.M. Lee, S.I. Lim, S.I. Kwun and Y.H. Jeong, Solid State Commun. 88 (1993) 361; D.J. Bae, T.Y. Koo, KB. Lee and Y.H. Jeong, Ferroelectrics 159 (1994) 91.
[33] H.S. Carslaw and J.C. Jaeger, Conduction of Heat in Solids, Clarendon Press, Oxford, 1959, p. 193.
[34] G. Arfken, Mathematical Methods for Physicists, Academic Press, Orlando, 1985, p. 488.
[35] This is, of course, a crude approximation neglecting the heat transfer between the two media. In an experimental situation dealing with a liquid, however, this approximation is not as bad as it may appear. For example, the thermal decay lengths of substrate glass and potassium-calcium nitrate liquid differ by only 20%.

[36] Y.H. Jeong and I.K. Moon, to be published.
[37] W. Nernst, Ann. Physik., 36 (1911) 395.
[38] H. Fujimori, Y. Adachi and M. Oguni, Phys. Rev., B46 (1992) 14501.
[39] For the approximate calculation of the shape factor and the heat conductance of gas, see F.M. Devienne, Adv. Heat Transfer 2 (1965) 276.
[40] H.Y. Ahn, S.Y. Jeong, I.K. Moon and Y.H. Jeong, J. Kor. Phys. Soc., 29 (1996) 5464.
[41] I.K. Moon and Y.H. Jeong, to be published in Pure & Appl. Chem. (1997).
[42] C. Moynihan et al., N.Y. Acad. Sci. 279 (1976) 15.
[43] Our method is called modified adiabatic, rather than adiabatic, calorimetry, since there is a heat flow from the sample to the shield. However, this heat flow is not a leak, but is used as a negative input power in a controlled fashion.
[44] W.H. Press, B.P. Flannery, S.A. Teukolsky, and W.T. Vetterling, Numerical Recipes in C, Cambridge University Press, Cambridge, 2nd edn., 1992, p. 650–655.
[45] J. Jäckle, Physica, A162 (1990) 377.